Letter of Intent for:

$\overline{\mathrm{P}}$ANDA

(AntiProton Annihilations at Darmstadt)

Strong Interaction Studies with Antiprotons

$\overline{\mathrm{P}}$ANDA Collaboration

January 8, 2004

We propose to study fundamental questions of hadron and nuclear physics in interactions of antiprotons with nucleons and nuclei, using the universal $\overline{\mathrm{P}}$ANDA detector. Gluonic excitations and the physics of strange and charm quarks will be accessible with unprecedented accuracy thereby allowing high-precision tests of the strong interaction. The proposed $\overline{\mathrm{P}}$ANDA detector is a state-of-the-art internal target detector at the *HESR* at *GSI* covering almost the full solid angle.

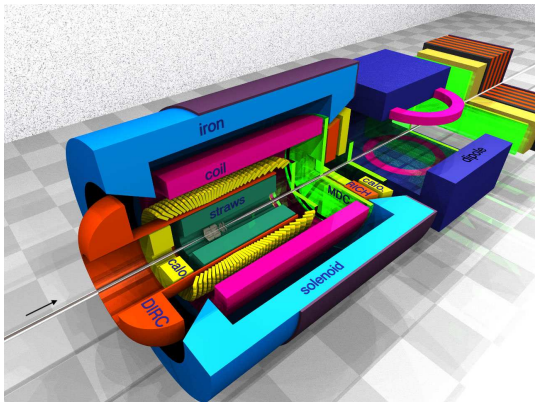

Figure 1: Artist's view of the $\overline{\mathrm{P}}$ANDA detector system for experiments at the internal target of the antiproton storage ring. It allows the detection and identification of neutral and charged particles generated within the relevant angular and energy range. This task will be shared by the combination of a central and a forward spectrometer of modular design which both are optimized for the specific kinematics of the antiproton-nucleon annihilation process.

The $\overline{\text{P}}$ANDA Collaboration

Universität Basel, Switzerland
M. Kotulla, B. Krusche, F. Zehr

Institute of High Energy Physics, Chinese Academy of Sciences, Beijing, China
J.J. Xie, B.S. Zhou

Universität Bochum, I. Institut für Experimentalphysik, Germany
T. Held, H. Koch, B. Kopf, B. Lewandowski, K. Peters, M. Steinke, A. Wilms

Helmholtz-Institut für Strahlen- und Kernphysik, Bonn, Germany
V. Credé, F. Hinterberger, H. Rohdjeß

Università di Brescia, Italy
A. Zenoni

Università di Catania and INFN-Laboratori Nazionali del Sud, Italy
F. Carace, M. De Napoli, G. Raciti, E. Rapisarda, L. Spezzi

Instytut Fizyki, Uniwersytet Jagiellonski, Cracow, Poland
P. Hawranek, B. Kamys, St. Kistryn, A. Magiera, P. Moskal, B. Piskor-Ignatowicz,
C. Piskor-Ignatowicz, Z. Rudy, P. Salabura, J. Smyrski, M. Wojciechowski

Gesellschaft für Schwerionenforschung mbH, Darmstadt, Germany
O. Hartmann, U. Lynen, H. Orth, T.R. Saitoh, C. Schwarz, C. Sfienti, A. Sokolov

Technische Universität Dresden, Germany
K.-T. Brinkmann, H. Freiesleben, R. Jäkel

Veksler-Baldin Laboratory of High Energies (VBLHE), Joint Institute for Nuclear Research ([a]),
Laboratory of Particle Physics (LPP) ([b]), Laboratory of Informative Technologies (LIT) ([c]), Joint
Institute for Nuclear Research, Dubna, Kabardian-Balkarian State University ([d]) and Institute of
Applied Mathematics and Automation ([e]), Nal'chik, Russia
A. Arefiev[a], M.Yu. Barabanov[a], B.V. Batyunya[a], D. Bogoslovski[a], T.Yu. Bokova[a], V.V. Borisov[a],
V.A. Budilov[a] Yu.V. Bugaenko[a], V.Kh. Dodokhov[a], A.A. Efremov[a], O.I. Fedorov[a], A.A. Feshchenko[b],
A.S. Galoyan[b], G. Ivanov[a], E. Jafarov[a], V.I. Kaplin[a], A. Karmokov[d], E.K. Koshurnikov[a],
V.Ch. Kudaev[e], V.I. Lobanov[a], A.F. Makarov[a], L.V. Malinina[a], K.V. Mikhailov[a], B. Morosov[a],
G.A. Mustafaev[d], A.M. Nakhushev[e], P.V. Nomokonov[a], I.A. Oleks[a], V. Pismennaya[a],
T.A. Pocheptsov[a], A. Polanski[c], A. Povtorejko[a], Yu.N. Rogov[b], I.A. Rufanov[a], S. Ryabtsun[b],
Z.Ya. Sadygov[a], R.A. Salmin[b], M.G. Sapozhnikov[b], T. Sereda[a], G.S. Shabratova[a], E.A. Strokovsky[b],
R.Sh. Teshev[d], V. Tikhomirov[a], E.P. Ustenko[a], V.V. Uzhinsky[c], N.V. Vlasov[b], P. Vlasov[a],
A.S. Vodopianov[a], S.A. Zaporozhets[a], A.I. Zinchenko[a]

University of Edinburgh, United Kingdom
M. Aliotta, D. Branford, K. Föhl, D. Watts, P. Woods

Friedrich Alexander Universität Erlangen-Nürnberg, Germany
W. Eyrich, A. Lehmann

Northwestern University, Evanston, U.S.A.
K. Seth

Università di Ferrara and INFN, Sezione di Ferrara, Italy
D. Bettoni, R. Calabrese, P. Dalpiaz, E. Luppi, M. Savriè

Johann Wolfgang Goethe-Universität Frankfurt, Germany
R. Dörner, R. Grisenti, M. Kaesz

INFN-Laboratori Nazionali di Frascati, Italy
P. Gianotti, C. Guaraldo, M. Iliescu, V. Lucherini, C. Petrascu, D. Sirghi, F. Sirghi

INFN, Sezione di Genova, Italy
R. Ballantini, M. Macri, R. Parodi, A. Pozzo

Justus Liebig-Universität Gießen, II. Physikalisches Institut, Germany
M.G. Destefanis, W. Döring, P. Drexler, M. Düren, I. Fröhlich, M. Hartig, D.G. Kirschner, W. Kühn, V. Metag, M. Nanova, R. Novotny, M. Pfeiffer, J. Ritman, C. Salz, S. Schadmand, J. Schneider, B. Seitz, H. Stenzel, U. Thöring

University of Glasgow, United Kingdom
J. Annand, A. Borissov, D. Ireland, R. Kaiser, J. Kellie, K. Livingston, C. McGeorge, D. Protopopescu, G. Rosner

Kernfysisch Versneller Instituut, Groningen, Netherlands
J. Bacelar, H. Löhner, J. Messchendorp

Institut für Kernphysik, Forschungszentrum Jülich, Germany
A. Gillitzer, D. Grzonka, V. Hejny, W. Oelert, D. Prasuhn, S. Sibirtsev, H. Ströher, P. Wintz

Uniwersytet Slaski, Katowice, Poland
J. Holeczek, J. Kisiel, B. Kłos,

Insitute of Modern Physics, the Chinese Academy of Science, Lanzhou, P.R. China
R. Chen, L. Duan, Z. Hu W. Li, Z. Sun, G. Xiao, Z. Xiao, H. Xu, H. Xu

Institut für Kernphysik, Johannes Gutenberg-Universität Mainz, Germany
P. Achenbach, J. Pochodzalla, A. Sanchez Lorente

Politecnico di Milano (^{a}), Physics Department, Università di Milano (^{b}) and INFN, Sezione di Milano (^{c}), Italy
P. Alberto^{b,c}, R. Bassini^c, C. Boiano^c, I. Iori^{b,c}, S. Riboldi^{a,c}

Research Institute for Nuclear Problems†, Belarus State University, Minsk, Belarus
V.I. Dormenev, G.Y. Drobychev, A.A. Fedorov, A.E. Korneev M.V. Korzhik, A.R. Lopatik, O.V. Missevitch

Technische Universität München, Germany
B. Ketzer, I. Konorov, S. Paul, L. Schmitt, Q. Weitzel

Westfälische Wilhelms-Universität Münster, Germany
D. Frekers, A. Khoukaz, A. Täschner, J. Wessels

Budker Institute of Nuclear Physics (BINP), Novosibirsk, Russia
E. Baldin, V. Malyshev, A. Maslennikov, S. Peleganchyk, G. Pospelov, A. Sukharev, Yu. Tikhonov

Dipartimento di Fisica Nucleare e Teorica, Università di Pavia (^{a}), INFN, Sezione di Pavia (^{b}), Italy
G. Bendiscioli^{a,b}, G. Boca^{a,b}, V. Filippini^b, A. Fontana^{a,b}, P. Genova^{a,b}, P. Montagna^{a,b}, A. Panzarasa^{a,b}, Alberto Rotondi^{a,b}, P. Salvini^b

Institute for High Energy Physics (IHEP)(^{a}), Protvino; Tomsk State University (TSU)(^{b}), Tomsk, Russia;
National Center of Particle and High Energy Physics (NCPHEP)(^{c}), Minsk, Belorussia
E. Ardashev^a, Yu. Arestov^a, G. Ayzenshtat^b, G. Britvich^a, B. Chuiko^a, S. Golovnya^a, S. Gorokhov^a, A. Kholodenko^a, V. Lishin^a, V. Parakhin^a V. Pikalov^a, V. Shelikhov^a, N. Shumeiko^c, A. Solinc^c, O. Tolbanov^b, A. Tyazhev^b, A. Vorobiev^a

Petersburg Nuclear Physics Institute of Academy of Science (PNPI), Gatchina, St. Petersburg, Russia
S. Belostotski, G. Gavrilov, Y. Naryshkin, O. Miklukho, A. Sarantsev, V. Vikhrov

Kungliga Tekniska Högskolan (KTH), Stockholm, Sweden
B. Cederwall, A. Johnson

Stockholms Universitet, Sweden
C. Bargholtz, K. Lindberg, P.E. Tegnér, I. Zartova

Università del Piemonte Orientale Alessandria, Torino and INFN, Sezione di Torino, Italy
M.L. Colantoni, L. Fava, D. Panzieri

Dipartimento di Fisica Generale 'A. Avogadro', Università di Torino and INFN, Sezione di Torino, , Italy
M. Alexeev, A. Amoroso, F. Balestra, R. Bertini, M.P. Bussa, O. Denisov, A. Ferrero, L. Ferrero, V. Frolov, R. Garfagnini, A. Grasso, A. Maggiora, M. Maggiora, G. Pontecorvo, G. Piragino, F. Tosello, G. Zosi

Dipartimento di Fisica Sperimentale, Università di Torino (^{a}), INFN, Sezione di Torino (^{b}), Politecnico

di Torino ([c]),Italy
M. Agnello[b,c], E. Botta[a,b], T. Bressani[a,b], D. Calvo[a,b], F. De Mori[a,b], A. Feliciello[a,b], A. Filippi[a,b], F. Iazzi[b,c], S. Marcello[a,b]

INFN, Sezione di Trieste and Università di Trieste, Italy
R. Birsa, F. Bradamante, S. Dalla Torre, M. Giorgi, A. Martin, P. Schiavon, F. Tessarotto

Physikalisches Institut, Universität Tübingen, Germany
H. Clement, E. Doroshkevitch, K. Ehrhardt, R. Meier

The Svedberg Laboratory, Uppsala, Sweden
H. Calén, C. Ekström, K. Fransson, A. Kupsc, P. Marciniewski

Uppsala Universitet, Sweden
F. Cappellaro, B. Höistad, T. Johansson, I. Lehmann, A. Lundborg, Ö. Nordhage, J. Nyberg, H. Pettersson, K. Schönning, P. Thörngren Engblom, U. Wiedner, J. Zlomanczuk

Institut für Mittelenergiephysik, Österreichische Akademie der Wissenschaften, Vienna, Austria
M. Cargnelli, H. Fuhrmann, P. Kienle, J. Marton, J. Zmeskal

Soltan Institute for Nuclear Studies, Warsaw, Poland
Z. Guzik, M. Kisielinski, T. Kozlowski, D. Melnichuk, B. Zwieglinski

Warsaw University of Technology, Institute of Atomic Energy, Otwock-Swierk, Poland
B. Slowinski

[†] Membership to be approved by the Coordination Board

Spokesperson: Ulrich Wiedner Email: ulrich.wiedner@tsl.uu.se
Deputy: Paola Gianotti Email: paola.gianotti@lnf.infn.it

Contents

1 Introduction

The accepted theory of the strong interaction is Quantum Chromodynamics (QCD). This theory is extremely successful in describing phenomena at high energies, where a clearly defined prescription exists how to use perturbation theory in order to accurately describe the interaction between quarks by the exchange of gluons, in close analogy to Quantum Electrodynamics (QED). In the energy regime of interest here, hadrons, being composite systems of quarks and gluons, become the relevant degrees of freedom. We enter the regime of strong coupling where astonishing new phenomena arise which represent open problems to date:

- Free quarks have not been observed, they seem to be confined within hadrons.
- The mass of hadrons is much larger than the summed mass of the quarks they are composed of.
- As a consequence of the characteristic self-interaction among gluons, glueballs and hybrids should exist. They consist predominantly of gluons or of glue and a quark-antiquark pair respectively.

All these phenomena are long-standing puzzles; they have their origin in the specific properties of the strong interaction, and represent a major intellectual challenge in our attempt to understand the nature of the strong force and the structure of multi-particle systems bound by this interaction. The complementarity between QCD and hadronic descriptions provides an ideal paradigm for one of the central issues of present day physics: the description of complex systems. In nearly all cases, different concepts are introduced for different levels of complexity and the challenge is to understand their relationship. For a number of processes both formalisms are applicable, permitting a systematic study of how quark-gluon and hadronic degrees of freedom are related.

2 Physics Case

Experimentally, studies of hadron structure can be performed with different probes such as electron, pion, kaon, proton or antiproton beams, each of which have its specific advantages. In antiproton-proton annihilation, particles with gluonic degrees of freedom as well as particle-antiparticle pairs are copiously produced, allowing spectroscopic studies with unprecedented statistics and precision. Antiprotons of 1–15 GeV/c will therefore be an excellent tool to address the open problems mentioned above. The following experiments are foreseen:

- Charmonium ($c\overline{c}$) spectroscopy: precision measurements of mass, width, decay branches of all charmonium states, especially for extracting information on the quark-confining potential. The unequaled resolution in the $\overline{\mathrm{p}}\mathrm{p}$ formation process and small systematic uncertainties give the unique opportunity to improve dramatically our knowledge which can not be achieved elsewhere.
- Firm establishment of the QCD-predicted gluonic excitations (charmed hybrids, glueballs) in the charmonium mass range (3–5 GeV/c^2) using high statistics in combination with sophisticated spin-parity analysis in fully exclusive measurements.
- Search for modifications of meson properties in the nuclear medium, and their possible relationship to the partial restoration of chiral symmetry for light quarks. Particular emphasis is placed on mesons with open and hidden-charm, which extends ongoing studies in the light quark sector to heavy quarks, and adds information on contributions of the gluon dynamics to hadron masses.
- Precision γ-ray spectroscopy of single and double hypernuclei for extracting information on their structure and on the hyperon-nucleon and hyperon-hyperon interaction.

As soon as the *HESR* facility reaches the full design luminosity further physics opportunities will open up like:

- Extraction of generalized parton distributions from $\overline{\mathrm{p}}\mathrm{p}$ annihilation,
- D meson decay spectroscopy (rare leptonic and hadronic decays), and
- Search for CP violation in the charm and strangeness sector (D meson decays, $\Lambda\overline{\Lambda}$ system).

Selected topics of the science case will be discussed in the following sections. For other topics not mentioned here, please refer to the CDR [1] and previous work on the physics and a potential detector [2, 3]. It is an important feature of the $\overline{\text{P}}$ANDA detector that for a given antiproton momentum and target selection, different physics aspects can be studied simultaneously.

2.1 Charmonium

The fundamental understanding of strong interactions in terms of QCD was greatly stimulated by the discovery of the J/ψ in 1974, this and other system of a charm and anti-charm quark (charmonium) ever since turned out to be a powerful tool in the understanding of the strong interaction. They are the results of $c\overline{c}$ spectroscopy which help tuning potential models of mesons. This is the place where the gluon condensate, which is closely related to the charmonium masses, is determined. It is the gluon condensate together with the $q\overline{q}$ condensate which represent the energy density of the QCD vacuum. The charmonium system offers unique advantages for understanding quarkonia, since the low density of states and their narrowness reduces mixing among them as long as they are below their corresponding open-charm thresholds.

So far the best understanding was achieved for the ψ states. These could be formed directly at electron-positron colliders. With an antiproton beam charmonium states of all quantum numbers could be formed directly and the precision of the mass and width measurement depends only on the beam quality. In this case the detector resolution is less important and the detector response is mainly optimized for an efficient background rejection. Important data on the excited non-ψ states, the D states of charmonium, will be extremely helpful to further develop theoretical understanding.

2.1.1 Narrow Charmonia

The comparison of the hadronic decays of the J/ψ and the ψ' [4] shows that radial excitations of charmonium are far from being simple recursions of the ground states. Therefore it is a necessity to identify and study the first radial excitation of the charmonium ground state η_c'. It was discovered by the *Belle*-Experiment in hadronic B decays [5] and was confirmed by *CLEO* and *Babar* [6] in $\gamma\gamma$-collisions. Its properties are incompatible with earlier findings by *Crystal Ball* [7] and is only marginally consistent with most model calculations. The accuracy for the width ($\Gamma = (19\pm10)\,\text{MeV}/c^2$) is only 50 %. Due to limited statistics and the systematical limitations of e^+e^- machines, including the measurements at the B-factories it is a $\overline{\text{p}}\text{p}$ scan which will finally settle these questions as it will be done as well for the ground state of charmonium, the η_c, where five very precise measurements of the η_c properties were performed in the past two years which disagree strongly among themselves [8].

The precision in the measurements will take advantage of the high yield of charmonium production in $\overline{\text{p}}\text{p}$ annihilations (e.g. $\text{BR}(\overline{\text{p}}\text{p} \to \eta_c) = (1.2 \pm 0.4) \times 10^{-3}$). By detecting hadronic final states ($KK\pi\pi$, $4K$, 4π, $K\overline{K}\pi$, $\eta\pi\pi$, ...) with branching fractions two orders of magnitude higher than in the $\gamma\gamma$ decay mode used so far, high-statistics samples can be easily collected.

The singlet-P resonance of charmonium, h_c, is of extreme importance in determining the spin dependent components of the $q\overline{q}$ confinement potential. Essentially nothing is known about it. A signal in the h_c region was once reported by *E760* in the process $\overline{\text{p}}\text{p} \to h_c \to J/\psi\pi^0$ [9]. This result needs confirmation in spite of the fact, that *E835* [10] took also data in this energy region and results are expected soon. It must be pointed out that due to the very narrow width ($\leq 1\,\text{MeV}/c^2$) and expected low yields, only a $\overline{\text{p}}\text{p}$ formation experiment like $\overline{\text{P}}$ANDA will be able to measure the h_c width and to carry out a systematic study of its decay modes. The proposed experiment could improve substantially the study of this state and is an important part of the charmonium program.

Many other aspects are worth measuring, like the radiative deexcitation of the χ_{cJ} states (^3P_J). These decays are dominated by the dipole term E1. Higher multipoles arise in the relativistic treatment of the interaction between the electromagnetic field and the quarkonium system, and can be studied by measuring the angular distributions of both χ_{c1} and χ_{c2}. A discrepancy with theory has been observed by the Fermilab experiments *E760* and *E835* [11, 12] at the $2.5\,\sigma$ level: further, high-statistics measurements are needed to increase the significance of the result.

2.1.2 States above the $D\overline{D}$ Threshold

Above the $D\overline{D}$ breakup threshold at 3.73 GeV/c^2 the charmonium spectrum is poorly known since e^+e^- experiments have only measured $R = \sigma(e^+e^- \to hadrons)/\sigma(e^+e^- \to \mu^+\mu^-)$ in large energy steps. Relatively washed-out structures were observed. The latest, much more accurate measurements by *BES* [13] do not confirm the sharp states reported by [14] and it is an open question if the higher vector states at 4040, 4160 and 4415 MeV/c^2 are in fact real. It is of critical importance to investigate this mass region in small energy steps. *E760/E835* were not able to study any physics above the $D\overline{D}$ threshold because of their energy limitation.

Yet this is the region in which narrow $^1D_2$, $^3D_2$ states (which are narrow because they cannot decay to $D\overline{D}$) and the first radial excitation of the h_c and the χ_{cJ} are expected to exist. A first evidence for such a state comes from *Belle* [15] and *CDF* [16] in the decay mode $J/\psi\pi^+\pi^-$. Its mass has been measured but does not fit easily in the current models. Therefore also other interpretations like a $D^0\overline{D}^{*0}$ molecule have been discussed. A precision measurement of all D states is mandatory to distinguish between various models.

In addition to the topics discussed above, exclusive charmonium decays represent a very interesting testing ground for QCD predictions. Of particular interest are hadron helicity non-conserving processes, G-parity violating decays, radiative ψ' decays and hadronic χ_{cJ} decays.

2.2 Gluonic Excitations and Exotics

The QCD spectrum is much richer than that of the naive quark model, as the gluons, which mediate the strong force between quarks, can also act as principal components of entirely new types of hadrons. These "gluonic hadrons" fall into two general categories: glueballs and hybrids. Glueballs are predominantly excited states of glue, while hybrids are resonances consisting largely of a quark, an antiquark and excited glue. The additional degrees of freedom carried by gluons allow glueballs and hybrids to have spin-exotic quantum numbers J^{PC} that are forbidden for normal mesons and other fermion-antifermion systems. Exotic quantum numbers (e.g., $J^{PC} = 0^{--}$, 0^{+-}, 1^{-+}, 2^{+-}) are the easiest way to distinguish gluonic hadrons from $q\overline{q}$ states, but even non-exotic glueballs and hybrids can be identified by measuring an overpopulation of the experimental meson spectrum and by comparing their properties (masses, quantum numbers, decay channels, etc.) with predictions from models or Lattice Quantum Chromodynamics (LQCD). Since the properties of glueballs and hybrids are determined by the long-distance features of QCD, their study will yield fundamental insights into the structure of the QCD vacuum.

The most promising results for gluonic hadrons in recent years come from antiproton annihilation experiments. Two particles, first seen in πN scattering [17, 18] with exotic $J^{PC} = 1^{-+}$ quantum numbers, $\pi_1(1400)$ [19] and $\pi_1(1600)$ [20] are clearly seen in $\overline{p}p$ annihilation at rest. In the search for glueballs a narrow state at 1500 MeV/c^2, discovered in antiproton annihilations by *Crystal Barrel* [21], is considered the best candidate for the glueball ground state ($J^{PC} = 0^{++}$). However, it mixes with nearby conventional scalar $q\overline{q}$ states, which makes the unique interpretation as glueball somewhat difficult.

2.2.1 Charmed Hybrids

Until now the search for glueballs and hybrids was mainly restricted to the mass region below 2.2 GeV/c^2. Because of the unavoidable problems due to the high density of normal $q\overline{q}$ mesons below 2.5 GeV/c^2 it would be experimentally very rewarding to go to higher masses, where the light quark states form a structureless continuum, and heavy quark states, which are far fewer in number, can easily be resolved. This is particularly true for the charmonium region. Exotic charmonia are expected to exist in the 3–5 GeV/c^2 mass region where they could be resolved and identified unambiguously.

Predictions for hybrids come mainly from calculations based on the bag model, flux tube model, and constituent gluon model and recently, with increasing precision, from LQCD [22, 23]. For hybrids, the theoretical results agree qualitatively, lending support to the premise that their predicted properties are not too far from reality. Charmonium hybrids can be expected since the effect of an extra gluonic degree of freedom in meson-like systems is evident in the confining potentials for the $c\overline{c}g$ system (e.g. as derived from LQCD calculations in the Born-Oppenheimer approximation [23]).

Until now, discussions have centered only around the lowest-lying charmonium hybrids. Four of these states ($J^{PC} = 1^{--}$, 0^{-+}, 1^{-+}, 2^{-+}) correspond to a $c\overline{c}$ pair with $J^{PC} = 0^{-+}$ or 1^{--}, coupled to a gluon

in the lightest mode with $J^{PC} = 1^{--}$. The other four states ($J^{PC} = 1^{++}$, 0^{+-}, 1^{+-}, 2^{+-}) with the gluon mode $J^{PC} = 1^{-+}$ are probably a bit heavier. Three of these eight charmonium hybrids have spin-exotic quantum numbers ($J^{PC} = 0^{+-}$, 1^{-+}, 2^{+-}), so mixing effects with nearby $c\overline{c}$ states are excluded, and experimental identification is especially easy. Compared to light hybrid candidates with reported widths of 200 to 400 MeV/c^2 [19, 20, 17, 18] charmonium hybrids are likely to be much narrower since open-charm decays are forbidden or suppressed below the $D\overline{D}^*_J$ +c.c. (often referred to as DD^{**}) threshold. From experiments at *LEAR* we know that production rates of such $q\overline{q}$ states are similar to those of states with exotic quantum numbers. We thus estimate that the cross sections for the formation and production of charmonium hybrids will be similar to those of normal charmonium states which is in the order of 120 pb ($\overline{\text{p}}\text{p} \to J/\psi\pi^0$ [24]), in agreement with theoretical predictions [25].

Formation experiments would generate non-exotic charmonium hybrids with high cross sections, while production experiments would yield a charmonium hybrid together with another particle, such as a π or an η. In $\overline{\text{p}}$p annihilation, production experiments are the only way to obtain charmonium hybrids with exotic quantum numbers. It is envisaged that the first step of exploring charmonium hybrids would consist of production measurements at the highest antiproton energy available ($E_{\overline{\text{p}}}$=15 GeV, $\sqrt{s}$=5.46 GeV/c^2), and studying all possible production channels available to cover exotics and non-exotic states. The next step would consist of formation measurements by scanning the antiproton energy in small steps in the regions in which promising hints of hybrids have been observed in the production measurements, thus having a second check on the static properties like the J^{PC} assignment as well as mass and width.

2.2.2 Glueballs

LQCD calculations make rather detailed predictions for the glueball mass spectrum in the quenched approximation disregarding light quark loops [26]. For example, the calculated width of approximately 100 MeV/c^2 [27] for the ground-state glueball matches the experimental results. In the mass range that is accessible to the *HESR* project, LQCD predicts the presence of about 15 glueballs, some with exotic quantum numbers.

Glueballs with exotic quantum numbers are called oddballs. These cannot mix with normal mesons; as a consequence, they are predicted to be rather narrow and easy to identify experimentally [28]. Since the spin structure of an oddball is different [28], it is conceivable that comparing oddball properties with those of non-exotic glueballs will reveal deep insights into the so-far unknown glueball structure. The lightest oddball, with $J^{PC} = 2^{+-}$ and a predicted mass of 4.3 GeV/c^2, would be well within the range of the proposed experimental program. Like charmonium hybrids, glueballs can either be formed directly in the $\overline{\text{p}}$p-annihilation process, or produced together with another particle. In both cases, the glueball decay into final states like $\phi\phi$ or $\phi\eta$ would be the most favorable reaction below 3.6 GeV/c^2 while $J/\psi\eta$ and $J/\psi\phi$ are the first choice for the more massive states.

The indication for a tensor state around 2.2 GeV/c^2 was found in the experiment of *JETSET* collaboration at *LEAR* [29]. The acquired statistics was not large enough and the complimentary reactions were not measured. We plan to measure the $\overline{\text{p}}\text{p} \to \phi\phi$ channel with statistics of two orders of magnitude higher than in the previous experiments. Moreover, other reactions of two vector particle production, such as $\overline{\text{p}}\text{p} \to \omega\omega, K^*\overline{K^*}, \rho\rho$ will be measured. On the other hand, the best candidate for the pseudoscalar glueball ($\eta_L(1440)$), studied comprehensively at *LEAR* by the *Obelix* collaboration [30], is not widely accepted to be a glueball signal only because the calculations of LQCD predict its mass above 2 GeV/c^2. Therefore, new data on many glueball states are needed to make a profound test of different model predictions.

It is worth stressing again that $\overline{\text{p}}$p-annihilations present a unique possibility to search for heavier glueballs, since alternative methods have severe limitations. The study of glueballs is a key to understanding long-distance QCD, so every effort should be made to identify them uniquely.

2.2.3 Other Exotics

Other exotics like tetra- and penta-quark systems (up to ≈ 2.7 GeV/c^2) are accessible as well in this energy range. Only charmed penta-quarks (if they exist) would require an antiproton beam of at least 20 GeV/c and are therefore not considered so far. Tetra-quark production can be investigated by Drell–Yan-like tagged events, where one $q\overline{q}$ pair creates a lepton pair, while the other four may produce a bound state of four quarks. The pentaquark production can be done near threshold (e.g. $\overline{\text{p}}\text{p} \to \Theta^+\overline{\Theta}^-$), where low partial waves dominate.

2.3 Charmed Hadrons in Matter

The investigation of medium modifications of hadrons embedded in hadronic matter is one of the main research activities at *GSI* at present and in the near future. The main physics goal is to understand the origin of hadron masses in the context of spontaneous chiral symmetry breaking in QCD and their modification due to chiral dynamics and partial restoration of chiral symmetry in a hadronic environment. Because of the limited energy available these studies have so far focused on the light quark sector. The in-medium potential of pions has been deduced from spectroscopic information obtained in the study of deeply bound pionic states [31]. Studies of K^+ production in proton-nucleus collisions [32] and of K^+ and K^- production in heavy-ion collisions [33, 34] are consistent with repulsive and attractive mass shifts of these particles, respectively, in nuclear matter. The study of medium modifications of the light vector mesons (ρ, ω, ϕ), for which substantial changes of spectral functions in the medium are predicted already at normal nuclear matter density [35], is the main research goal of the *HADES* experiment.

A high-intensity $\overline{\mathrm{p}}$ beam up to 15 GeV/c will allow an extension of this program to the charm sector, both for hadrons with hidden- and open-charm. The short-distance interaction of charmonium states, consisting of charm quarks only, with color singlet hadrons is governed by the exchange of two or more gluons. As the masses of charmonia are dominated by the large mass of the charm quark pair, only little sensitivity to changes in the quark condensate is expected for charmonium states. Consequently, the in-medium mass of these states would be affected primarily by a modification of the gluon condensate. Investigating the interaction of $c\overline{c}$ mesons with nucleons and nuclei is therefore a way to exploring fundamental aspects of gluon dynamics in QCD. For the low-lying charmonium states J/ψ and η_c recent calculations [36] indicate, however, only small in-medium mass reductions of the order of 5–10 MeV/c^2, but since this effect is expected to scale with the volume occupied by the $c\overline{c}$ pair, the situation may be different for excited charmonium states. Large attractive mass shifts of 40 MeV/c^2 for χ_{cJ}, 100 MeV/c^2 for ψ', and 140 MeV/c^2 for $\psi(3770)$ were recently predicted by modeling a QCD 2^{nd} order Stark-effect [37].

For D mesons, the situation is different. Built of a heavy c quark and a light antiquark, the D meson is the QCD analogue to the hydrogen atom. Hence, D mesons provide the unique opportunity to study the in-medium dynamics of a system with a single light quark. Recent theoretical work agrees in the prediction of a mass splitting for D mesons in nuclear matter, but disagrees in the predicted size of the splitting (50 MeV/c^2 in Ref. [38, 39], 160 MeV/c^2 in Ref. [40]) and in the sign of the D^- mass shift (attractive in Ref. [38, 39], repulsive in Ref. [40]).

To date, very little experimental information is available on charm propagation in nuclear matter, and theoretical predictions are highly model dependent. Therefore, in order to form a basis for a better understanding of the behavior of charmed hadrons in nuclear matter, first studies within this program should concentrate on the measurement of J/ψ and D meson production cross sections in $\overline{\mathrm{p}}$ annihilation on a series of nuclear targets. The comparison of the resonant J/ψ yield obtained from $\overline{\mathrm{p}}$ annihilation on protons and different nuclear targets allows to reliably deduce the J/ψ nucleon dissociation cross section [41]. This is not only interesting in its own right, but also particularly important for the understanding of J/ψ suppression in ultra-relativistic heavy-ion collisions, interpreted as a signal for a transition to a quark-gluon phase.

In particular, an exclusive measurement of the final states populated in $\overline{\mathrm{p}}$d collisions would allow to determine the coupling between different channels with charmed hadrons, and to study the interaction of charmed hadrons with nucleons and mesons in the final state. For example, the reaction $\overline{\mathrm{p}}\mathrm{d} \rightarrow J/\psi\gamma\mathrm{n}$ [42] provides the possibility to measure the elastic $J/\psi + N$ cross section down to low relative momenta.

The experimental access to medium modifications of charmed hadrons is more difficult. Whereas the in-medium mass of charmonia can be reconstructed from their decay into di-leptons or photons, different signals have been proposed for the detection of the in-medium mass shifts of D mesons. A reduction of the $D\overline{D}$ threshold would result in an increased D and $\overline{D}$ production in $\overline{\mathrm{p}}$ annihilation on nuclei particularly at subthreshold energies [40]. D and $\overline{D}$ mesons can be identified via their hadronic decays with $\overline{K}$ and K mesons in the final state. Cross sections of typically 1 nb near threshold lead to about 100 events registered per day at a luminosity of $2\times10^{31}\,\mathrm{cm}^{-2}\mathrm{s}^{-1}$ which would allow a substantial D meson physics program.

Moreover, a lowering of the $D\overline{D}$ threshold in the nuclear medium could open this decay channel or increase its partial width for the decay of the excited charmonium states lying close to the free $D\overline{D}$ mass ($\psi(3770)$, ψ', χ_{c2}) [39], provided the reduction of the in-medium masses of the charmonium states is sufficiently small. Recent model calculations [43] indicate that a dropping of the $D\overline{D}$ threshold in the nuclear medium by ~ 50MeV/c^2 could be seen in a suppression of low-mass dileptons from the decay of

the $\psi(3770)$.

2.4 Hypernuclei and Di-Baryons

Replacing an up or a down quark with a strange quark in a nucleon which is bound in a nucleus, leads to the formation of a hypernucleus. A new quantum number, strangeness, is then introduced into the nucleus, adding a third axis to the nuclear chart. Due to experimental limitations this third dimension has been scarcely explored. The hyperon – usually a Λ particle – is no longer restricted by the Pauli principle for populating all the possible nuclear states as neutrons and protons are. It may occupy all the allowed single-particle states without the complications encountered in ordinary nuclei, like pairing interactions. Describing the pure single-particle states by well known wave functions, one may extract the strength of the Λ-N strong interaction and analyze furthermore its decomposition into the different spin-dependent contributions, with significantly different predictions from meson exchange or quark models. At the same time also the Λ-N weak interaction can be studied where the Pauli principle acts in the opposite sense: the decay of the Λ into $N\pi$, is suppressed, since all the nucleon states in the nucleus are already occupied; on the contrary the process $\Lambda N \rightarrow NN$ is allowed, opening an unique window of this four-baryon, strangeness non-conserving interaction.

Single and double Λ-hypernuclei were discovered 50 years [44] and 40 years ago [45], respectively. However, only 6 double-Λ hypernuclei are known up to now, in spite of a considerable experimental effort in the last 10 years. Thanks to the use of $\overline{p}$ beams and the clever combination of experimental techniques, a copious production at $\overline{\text{P}}$ANDA is expected, even more than at (planned) dedicated facilities. A new chapter of strange nuclear physics will be then opened, whose first result will be the determination of the $\Lambda\Lambda$ strong interaction strength, definitively not possible with direct scattering experiments. The possible existence of an S = -2 six-quark ($uuddss$) H-di-baryon [46] represents another challenging topic of $\Lambda\Lambda$ hypernuclear physics. So far the experimental searches for this lightest strangelet are inconclusive, moreover even a strongly bound H can not be excluded [47]. In fact the short time scale, of the order of 10^{-23} s, available in a coalescence process may prevent the transition from a $\Lambda\Lambda$ state to an H-particle in free space. Here, double-Λ hypernuclei may serve as "catalyst" for the H-particle: the long lifetime, of the order of 10^{-10} s, of two Λ's bound together in a nucleus may help to overcome a possible repulsive interaction at short distances. Since the mass of the H-particle might drop inside a nucleus [48] and due to hyperon mixing [49] it might be possible to observe traces of the H. Thus spectroscopy of S = -2 hypernuclei can give important information on this fascinating object. Finally, hyperatoms created during the capture process of the hyperon will supply new information on fundamental properties of the hyperons. For example, the Ω^- is the only baryon whose *static* quadrupole moment can be determined experimentally [50]. At *HESR* the large number of produced Ω^--atoms will enable us to determine the hyperfine splitting in an Ω^--atom and thus - for the first time - provide information on the static deformation of a baryon.

Until the end of the last decade, the energy resolution on hypernuclear levels observed with electronic detectors was limited to typical values of about 1 MeV. Only recently high-efficiency Ge-arrays opened the door to high resolution γ-ray spectroscopy. In combination with the high luminosity foreseen at *HESR* and with a novel solid-state micro tracker, high resolution γ-ray spectroscopy of double hypernuclei and Ω-atoms will become possible for the first time. In order to minimize the background from associated particles, the production of hypernuclei and hyperatoms at *HESR* will rely on $\Xi\overline{\Xi}$ and $\Omega\overline{\Omega}$-pair production close to threshold in $\overline{p}$-nucleus collisions. The trigger will be based on the detection of a high momentum anti-hyperons at small angles or of positive kaons produced by the anti-hyperons absorbed in the primary target nuclei. The $2\,K^+$ trigger will provide significantly higher count rates but requires the detection of rather low momentum kaons of a few hundreds MeV/c. The second ingredient of the experiment is the deceleration of the Ξ^- inside the nucleus and subsequent absorption in an secondary active target. The geometry of this secondary absorber is determined by the short mean life of the Ξ^- of only 0.164 ns. If the separation between the primary target and the secondary absorber is too large, low momentum Ξ^- will decay prior to full stopping. On the other hand, energetic Ξ^- with momenta beyond approximately 500 MeV/c can not be stopped prior to their decay. This limits the required thickness of the active secondary target to about 30 mm. In order to track the stopped Ξ^- and the charged fragments resulting from the decay of the produced hypernuclei, it is planned to sandwich the absorber with solid state pixel or strip detectors. Finally an efficient Ge γ-ray detector is required. The main limitation will be the load of associated particles (100 kHz for each detector element). Since most of the produced particles are emitted in the forward region not covered by the Ge-array, an interaction rate of a few 10^7/s seems to be manageable. With these three ingredients it will be possible to reconstruct approximately 3000 stopped

Ξ^- (with the unique $\overline{\Xi}^+$ tag) per day at $\overline{\mathsf{P}}$ANDA. By requiring kaons, this number will be increased by up to two orders of magnitude. The rate could be much smaller for Ω-atoms ($\sigma_{\Omega\overline{\Omega}} \approx 0.1\,\mu$b). Although X-ray spectroscopy for Ω-atoms could be feasible with *HESR* and $\overline{\mathsf{P}}$ANDA, the rate and production mechanism still need further investigation. This experiment will also benefit from studies of antiprotonic atoms at the proposed low energy antiproton facility *FLAIR* [51] at *GSI*.

2.5 Electromagnetic Processes

2.5.1 Crossed-Channel Compton Scattering and Related Exclusive Processes

The theoretical framework of Generalized Parton Distributions (GPDs) [52, 53], which has been developed only a few years ago [54, 55], caused a lot of excitement in the field of understanding the structure of the nucleon in the terms of QCD. It has recently been shown that exclusive $\overline{\mathrm{p}}\mathrm{p}$ annihilation into two photons at large s and t can also be described in terms of GPDs [56, 57, 58]. Using the handbag diagram, the process is separated into a 'soft' part which is parameterized by GPDs and a 'hard' part which describes the annihilation of a quasi-free $q\overline{q}$ pair into two photons. Estimates of the expected count rates based on a simple model predict a few thousand $\gamma\gamma$-events per month for a luminosity of $2 \times 10^{32}\mathrm{cm}^{-2}\mathrm{s}^{-1}$ at an energy of $\sqrt{s}$ =3.2, GeV/c^2 [59]. Other estimates, based on cross section measurements of the inverse process $\gamma\gamma \to \overline{\mathrm{p}}\mathrm{p}$ predict count rates which are up to a factor 50 [60, 61] above the estimate of [59] but still are consistent with the handbag ansatz. The experiment *E760* at Fermilab has measured already the process $\overline{\mathrm{p}}\mathrm{p} \to \gamma\gamma$ at various angles, however the measured count rates were completely dominated by background from processes like $\overline{\mathrm{p}}\mathrm{p} \to \pi^0\pi^0$ [62].

It is proposed to measure the crossed-channel Compton scattering and the related exclusive annihilation processes with a scalar meson, a vector meson or a lepton pair in the final state at the $\overline{\mathsf{P}}$ANDA experiment [63]. The comparison of the differential cross sections of the various processes and the comparison with GPD based models will allow new insights into the annihilation process in terms of quark models and QCD.

2.5.2 Transverse Quark Distributions and Drell–Yan Processes

Historically, the first extensive discussion of transverse spin effects in high energy hadronic physics followed the discovery of a large transverse polarization for Λ-hyperons, produced in pN interactions at relatively high p_T in 1976 [64]. Transverse polarization of quarks is not probed in deeply inelastic scattering (DIS), but can be studied in other hard reactions as semi-inclusive lepto-production or Drell–Yan di-muon production. At leading twist level, the quark structure of hadrons is described by three distribution functions:

- the unpolarized function $f(x)$, which is the probability of finding a quark with a fraction x of the longitudinal momentum of the parent hadron, regardless of its spin orientation;
- the longitudinal polarization distribution $\Delta f(x)$, that measures the net helicity of a quark in a longitudinally polarized hadron;
- the transverse polarization $\Delta_T f(x)$, which is the number density of quarks with transverse polarization in a transversely polarized hadron

Model calculations show that [65], at least at low Q^2, $\Delta f(x)$ and $\Delta_T f(x)$ are of the same order of magnitude. However QCD evolution is quite different and, at low x, $\Delta_T f(x)$ turns out to be suppressed with respect to $\Delta f(x)$. Moreover $\Delta_T f(x)$ has no gluonic counterpart in spin 1/2 hadrons: the gluon transversity distributions for nucleons does not exist.

The experimental information on $\Delta_T f(x)$ is very poor. This is because transversity distributions are not observable in fully inclusive DIS, the reaction that provided the largest amount of the existing data on structure functions. Data on transversity are presently collected by *COMPASS* on some semi-inclusive DIS and *HERMES*. But $\Delta_T f(x)$ can only be extracted by unfolding the data with fragmentation functions obtained from other experiments. Much easier is the study of quark transverse polarization via Drell–Yan lepton pair production in pp or $\overline{\mathrm{p}}\mathrm{p}$ collisions because the transverse quark distributions appear at leading twist level and the cross sections contain no unknown quantities besides the transversity distributions themselves. This makes theoretical predictions easier with respect to the other reactions.

The $\overline{\mathrm{p}}\mathrm{p} \to \mu^+\mu^- X$ reaction has the same scaling properties as pp, which favors the lowest beam energy consistent with the di-muon mass produced in the "safe" region between the $c\overline{c}$ and the $b\overline{b}$ bound states. Thus it is an ideal tool to study nucleon structure functions. From the data of [66], where $\overline{\mathrm{p}}\mathrm{p} \to \mu^+\mu^- X$ has been studied at a beam momentum of 125 GeV/c and for di-muon masses between 4 and 6 GeV/c^2 one can expect an absolute cross section integrated over positive x_F and all transverse momenta of about 0.6 nb at 20 GeV/c. Since the "safe" region is limited to less than 6 GeV/c^2 the utilization of the maximal available energy of the produced antiprotons is envisaged. The measurement of spin observables of the reaction $\overline{\mathrm{p}}\mathrm{p} \to \Lambda\overline{\Lambda}$, taking advantage of the self-analyzing power of the Λ ($\overline{\Lambda}$), is also of greatest interest because it provides the check of the factorization approach and contains the products of the structure and fragmentation functions.

2.5.3 Electromagnetic Form Factors of the Proton in the Time-like Region

The electromagnetic form factor of the proton in the timelike region can be extracted from the cross sections for the process $\overline{\mathrm{p}}\mathrm{p} \to e^+e^-$. First order QED predicts:

$$\frac{d\sigma}{d\cos\theta^*} = \frac{\pi\alpha^2\hbar^2c^2}{2xs}\left[|G_M|^2(1+\cos^2\theta^*) + \frac{4m_p^2}{s}|G_E|^2(1-\cos^2\theta^*)\right]$$

with G_E and G_M the electric and magnetic form factors, respectively. Data at high Q^2 are crucial to test their Q^2 behavior and the space-like–time-like equality for corresponding Q^2.

The proton timelike form factors have been measured by several experiments in the low Q^2 region down to threshold. At high Q^2 the only measurements have been achieved by *E760* and *E835* at Fermilab [67] up to $Q^2 \approx 15\,\mathrm{GeV}^2/c^2$. However, due to limited statistics G_M and G_E have not been measured separately and could only be extracted using the assumption $G_E = G_M$.

A measurement over the widest Q^2 range ever covered by a single experiment is envisaged - from threshold to 20–25 GeV$^2/c^4$ or above. Due to much higher statistics it will be possible to measure G_M and G_E separately. This measurement will not require dedicated running, but will be carried out parasitically to the charmonium and charmed hybrid program.

2.6 Open-Charm Physics

HESR running with full luminosity (limited by the production rate of $2\times10^7\,\overline{\mathrm{p}}$/s) at momenta larger than 6.4 GeV/c would produce large numbers of D meson pairs. Such an installation can be considered as a hadronic factory for tagged open-charm, with about 100/ s charmed pairs around $\psi(4040)$. Despite the small ratio (5×10^{-6}) of charm production to total cross section, the background conditions are expected to be favorable because the hadrons are produced at threshold with no room for additional hadrons in the same process. The high yield and the well defined production kinematics of D meson pairs allows to investigate e.g. D and D_s and their broad physics spectrum.

2.6.1 D and D_s Spectroscopy

The B-Factory experiments have discovered several resonances in the D ($c\overline{d}$, $c\overline{u}$ and c.c.) and D_s ($c\overline{s}$ and c.c.) sector with two of them extremely narrow ($D^*_{sJ}(2317)$ [68] and $D_{sJ}(2458)$ [69]). These measurements have triggered a lot of discussion, since they appear at unexpected locations giving rise to speculations about their actual nature. The large mass shift (compared to theoretical predictions [70]) is discussed in terms of chiral aspects in heavy-light systems [71]. This model would have strong implications on any system with a single light quark. Although there is some evidence for the scalar D-state [72] it is important to verify this finding and to settle down this question. Threshold pair production can be utilized to get very precise measurements of the mass and the width of excited D and D_s states.

2.6.2 Rare Decays

The study of rare decays can open a window to physics beyond the standard model since it probes symmetry violation. Lepton flavor number violating decays, e.g. $D^0 \to \mu e$ or $D^\pm \to \pi\mu e$, are interesting to search for. Flavor changing neutral currents like in the decay $D^0 \to \mu^+\mu^-$ can occur in the standard model through box graphs or weak penguin graphs with branching fractions smaller than 10^{-15}. However

the signatures of these decays are clean leaving hope for their observation, if processes exist boosting the decay branch.

2.6.3 CP Violation

CP violation [73] has been observed in neutral kaon and in neutral B meson decays [74, 75]. In the standard model, CP violation arises from a single phase entering the CKM matrix. As a result, two elements of this matrix, i.e. V_{ub} and V_{td} have large phases. Because these elements have small magnitudes and involve the third generation, CP violation is small in the K^0 system and is predicted to be even smaller in the D^0 system [76]. Thus, a deviation from the small standard model effect indicating "new physics" can be more easily distinguished in experiments in the D meson system.

Working with D mesons produced at the $D\overline{D}$ threshold has also some advantages arising from the strong correlation of the $D\overline{D}$ pair, which is kept in the hadronization process. Formed near threshold, no asymmetries are expected in the production process, and the observation of one D meson tells about the quantum numbers of the other one when produced in a charge symmetric environment (flavor tagging). Thus flavor ($D\overline{D}$) mixing and CP violation can be searched for in analogy to methods in the B-system produced on the $\Upsilon(4S)$ [77].

3 $\overline{\text{P}}$ANDA Detector

3.1 Requirements

The rich experimental program being proposed in the previous section can only be pursued with a universal hermetic modular detector which is capable of detecting charged and neutral particles with nearly 4π solid angle coverage and high resolution. The basic elements are:

- Hidden-charm physics and the search for exotics require the concurrent detection of di-lepton pairs as well as good kaon identification and high efficiency for open-charm final states. In addition the detection of low energy photons, either from radiative decays and/or background channels, is extremely important. Thus, muon detection capabilities and a highly-segmented low-threshold electromagnetic calorimeter are important to tag and precisely reconstruct hidden-charm and to reduce background. Good vertex recognition and particle identification for charged kaons from very low energies up to a few GeV/c is mandatory to reconstruct light hadronic and open-charm final states.

- The detector must withstand large radiation dosage from hadrons emmitted from the spallation process when using nuclear targets. These spallation products include neutrons down to thermal energies, which contribute most.

- The specific demands for experiments with a secondary target require a good detection of antihyperons and low momentum K^+ in the forward region. A compact high-resolution solid state tracker for absorption and tracking of low momentum hyperons at large angles is certainly needed. The geometry of this secondary target is determined by the short mean life of the Ξ^- of only 0.164 ns. To measure the radiative transitions a high resolution and high-efficiency Ge-array for γ-ray detection is envisaged.

- Open-charm spectroscopy and electromagnetic reactions have similar demands as are envisaged in the hidden-charm and exotics programs (see chapter 2.1.2 and 2.2). It is worthwile to mention that the decay of a charmed hadron releases a rather high p_t (up to 1.5 GeV/c) as compared to light and even strange meson decays. This leads to large opening angles of the daughter particles in the laboratory reference frame.

3.2 Overview

For the envisaged experimental program a nearly full coverage of the solid angle together with good particle identification and high energy and angular resolutions for charged particles and photons are mandatory. The proposed detector is subdivided into the target spectrometer (TS) consisting of a solenoid around the interaction region and a forward spectrometer (FS) based on a dipole to momentum-analyze

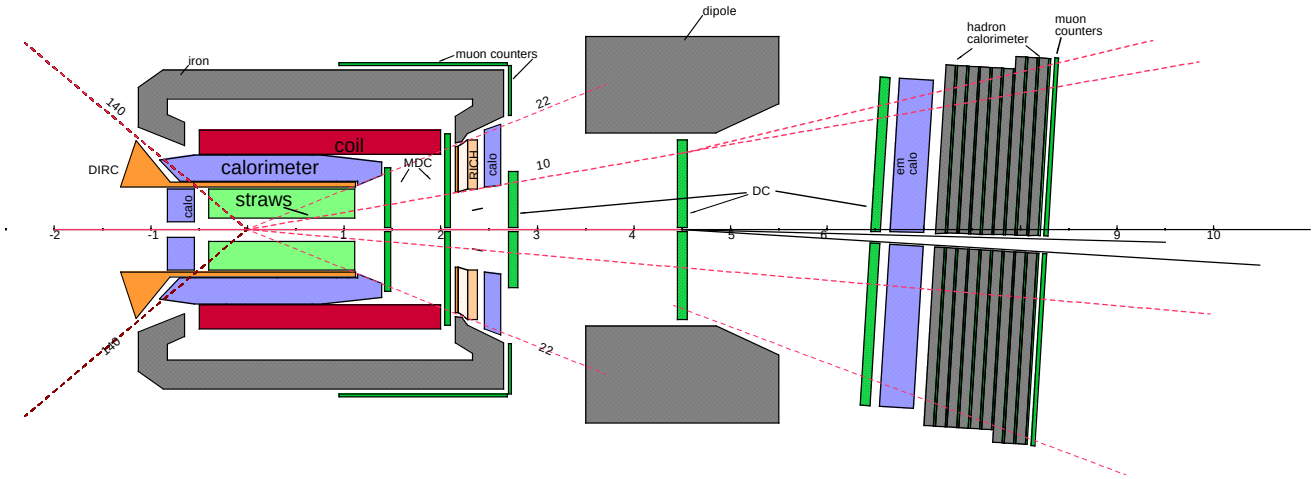

Figure 2: Schematic overview of the detector facility from above.

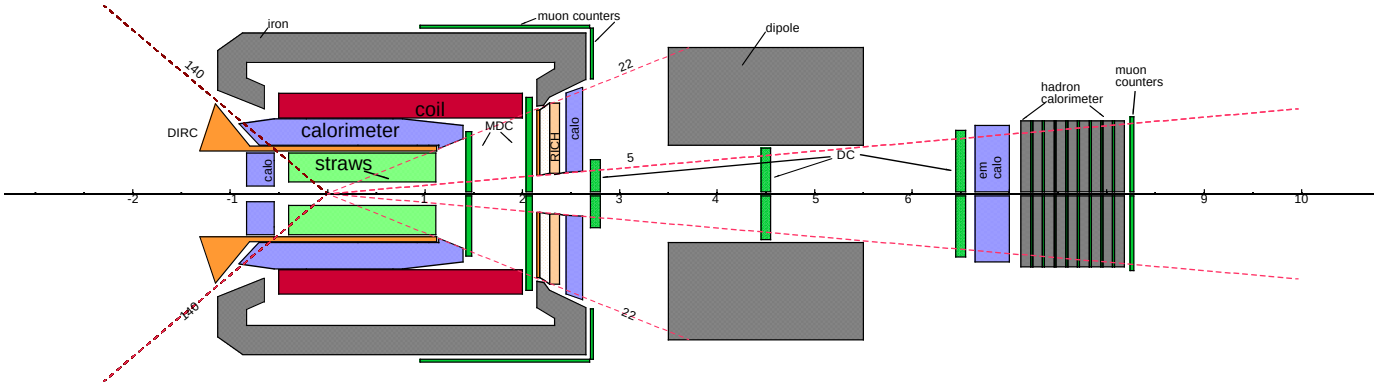

Figure 3: Schematic overview of the detector facility from the side.

the forward-going particles (see fig.3.2 and 3.2). The combination of two spectrometers allows a full angular coverage, it takes into account the wide range of energies and it still has sufficient flexibility, so that individual components can be exchanged or added for specific experiments, e.g. for the experiments with hypernuclei or for the special needs of CP violation studies.

Particles emitted with laboratory polar angles larger than 5° are measured solely in the TS. Surrounding the interaction volume there will be 4 diamond or silicon start detectors (each $20\times30\,\text{mm}^2$) followed by 5 layers of a silicon micro-vertex detector. Starting from a radial distance of 15 cm from the beam line, up to 42 cm, there will be 15 double-layers of crossed straw tubes, that extend from 40 cm upstream to 110 cm downstream of the target. At a radial distance of 45 cm a cylindrical DIRC follows. The forward region will be covered by an aerogel Cherenkov detector using proximity focusing onto gas based photon detectors. These detectors are surrounded by an electromagnetic calorimeter consisting of $PbWO_4$ crystals that are read out with avalanche photodiodes. In the region between the calorimeter and the end-cap there will be two sets of mini drift chambers. The TS is contained in a 2.5 m long and 90 cm radius solenoid. Behind the return yoke there will be scintillating bars for muon identification.

Particles emitted with polar angles below 10° in the horizontal and 5° in the vertical direction are measured with the help of a 1 m gap FS-dipole. MDCs will be located before and behind the dipole for tracking. Particle identification will be obtained by a TOF-Stop detector and a dual-radiator RICH detector. Behind this there is a $3\,\text{m}^2$ lead glass calorimeter and a hadronic calorimeter followed by a muon detection system.

3.3 Target Spectrometer

3.3.1 Target System

In many experiments using internal targets in a storage ring, gas, cluster-jet or wire targets have been used. All target types including also alternative developments in the recent past have at present their particular advantages and problems. Therefore we will investigate several target options. A decision about which target to be used for which physics question has to be answered after the R&D phase has been completed.

The basic geometrical properties considered for the internal target are the diameter of the beam pipe and the target mandrel which are 20 mm at the intersection. The mandrel opens up gradually reaching 100 mm outside the calorimeter and 350 mm through the iron yoke. The beam pipe opens up in backward direction to 140 mm diameter, in order to provide sufficient pumping power. In downstream direction it stays at 20 mm diameter until the end of the vertex tracker.

This setup will allow different internal targets. Currently a pellet target and cluster-jet targets are developed to fit inside the target chamber. Given a stored number of 10^{11} antiprotons in the *HESR* a target density of 5×10^{15} hydrogen atoms per cm^2 is required to reach the design luminosity.

Cluster-Jet Target To fulfill this demand with a cluster-jet target requires a density increase of one order of magnitude compared to what has presently been achieved. In addition, due to detector constraints, the distance between the cluster-jet nozzle and the target has to be increased compared to other applications. The size of the target region will be given by the lateral spread of hydrogen clusters, which, when optimized, should stay less than 10 mm. The great advantage of cluster targets is the homogenous density profile and the possibility to focus the antiproton beam at highest phase space density. Hence the interaction point is defined transversely but has to be reconstructed longitudinally in beam direction. The possibility to adjust the target density along with the gradual consumption of antiprotons for running at constant luminosity is an advantage while the badly defined interaction-point is a problem for any open-charm measurement. Internal cluster targets can run with other gases as well. So not only hydrogen but also nuclear targets will be provided by this target technique.

Pellet Target Another internal target consists of a stream of frozen hydrogen micro-spheres, called pellets, traversing the antiproton beam perpendiculary. The design will be based on the pellet target placed inside the 4π *WASA* detector at the *CELSIUS* storage ring [78]. At the interaction point, typical parameters are a pellet rate of 10-15 kHz, a fall speed $\gtrsim$60 m/s and a pellet size of 25–35 μm, which together imply a target thickness of a few 10^{15} atoms/cm^2. Due to the angular divergence of the pellets, the projected circle area has diameter $\lesssim$3 mm. Since a single pellet undergoes about 100 interactions during the time it traverses the beam, it will be no difficulty to determine the position of individual pellets with the necessary accuracy not only in transverse but also longitudinal direction. For $\overline{\mathsf{P}}$ANDA, the present performance of the *WASA* pellet target needs to be improved. The ongoing further development of the target at a dedicated test area at *CELSIUS* is expected to improve the present performance both in pellet rate and size. Moreover, the production of deuterium pellets has to be established, and the use of even heavier targets is to be envisaged.

Other Targets Concerning nuclear targets a technique with fibers or wires may be used. The excellent beam emittance of better than 1 mm mrad can be expected for the *HESR* to be exploited best. While problems with beam heating apply also for fiber or wire targets, they pose no additional constraints on the detector system.

3.3.2 Micro Vertex Detector

The design of the microvertex detector (MVD) for the target spectrometer at *HESR* is optimized for the detection of secondary vertices and maximum acceptance close to the interaction point. It will also strongly improve the transverse momentum resolution. In addition a layer of diamond or Si detectors can provide a start signal.

The concept of the MVD is based on radiation hard silicon pixel detectors with fast individual pixel readout circuits. The layout foresees a five layer barrel detector with an inner radius of $\gtrsim$1 cm and an

outer radius of 6 cm. It will have 7.2 million pixels of $50\times300\,\mu\text{m}^2$ size. For optimal vertex resolution in both azimuthal and longitudinal direction, the pixels will be arranged longitudinally for the inner three layers, and azimuthally for the outer two layers. Five detector layers arranged perpendicular to the beam will give best acceptance for the forward part of the particle spectrum. This detector part contains about two million pixels with $100\times150\,\mu\text{m}^2$ size. All detector wafers are $200\,\mu$m thick ($0.25\%\,X_0$).

The readout via bump-bonded wafers with ASICs as it is used in *ATLAS* and *CMS* [79, 80] is foreseen as the default solution. It is highly parallelized and allows zero suppression as well as the transfer of analog information at the same time. The readout wafer has a thickness of $300\,\mu$m ($0.37\%\,X_0$). An alternative readout scheme is presently in development for future high energy experiments and has already been used in X-ray astronomy [81]. Active pixels contain the charged particle sensitive part on one side and implement each pixel's readout circuit on the other side of the same silicon wafer. The clear advantage is that only half of the material thickness has to be used for the same detection capability, which reduces multiple scattering and secondary interactions.

3.3.3 Tracking Detectors

The charged-particle tracking devices must handle the high particle fluxes that are anticipated for luminosities of up to $2\times10^{32}\,\text{cm}^{-2}\text{s}^{-1}$. The momentum resolution $\delta p/p$ should typically be on the percent level and the detectors should have a good detection efficiency for secondary vertices which can also occur outside the inner vertex detector (e.g. K^0_S or Λ). This can be achieved by the combination of the vertex detectors, a cylindrical arrangement of straws at large angles, and two sets of 8 (or 6) layer mini drift chambers, similar to those developed for the *HADES* experiment at *SIS18*.

Straw Tube Tracker In total there are 15 double-layers of straws at radial distances between 15 cm and 42 cm to the beam and their overall length is 150 cm. The first and last double-layers are arranged parallel to the beam axis, and the remaining 13 double layers are arranged at skew angles ranging from 4.5° to 9°. The skew angles cause the stereo layers to form a hyperboloidal shape and allow to determine the position of the particles along the beam direction to about 1 mm. In order to remove the left-right ambiguity the straws are assembled in double-layers which are packed into supports of Al-Be semi-rings. The straws have diameters ranging from 4 mm (innermost) to 8 mm (outermost). The tube wall will have a thickness of about $30\,\mu$m (aluminized mylar, or carbon loaded kapton). As sense wires $20\,\mu$m thick gold plated tungsten wires are foreseen. The amount of material could be minimized by self-supporting tubes held by a light Al-Be mechanical frame. The gas mixture used will be Argon based with CO_2 as quencher. We foresee to have a gas gain not greater than 10^5 in order to guarantee long term operation. With these parameters, we expect a resolution in x and y coordinates of about $150\,\mu$m.

Mini Drift Chambers Particles emitted at angles below 22° which are not covered fully by the Straw Tube Tracker will be tracked with two multi-wire drift chambers (MDC) placed 1.4 m and 2.0 m downstream of the target. The chambers have to stand a high counting rate of particles peaked at the most forward angles due to the relativistic boost of the reaction products as well as due to the small angle $\overline{\text{p}}$p elastic scattering. With the envisaged luminosity the expected particle flux in the first chamber in the vicinity of the 5 cm diameter beam pipe is about $2\times10^4\,\text{cm}^{-2}\text{s}^{-1}$. Besides, the chambers have to work in the 2 T magnetic field produced by the $\overline{\text{P}}$ANDA-solenoid.

In order to fulfill these requirements quadratic (or hexagonal) drift cells with an area of $1\,\text{cm}^2$ were chosen. Each chamber will contain several pairs of detection planes. The number of pairs and their orientation will depend upon the actual symmetry (quadratic or hexagonal). The planes in each pair will be staggered by half of the cell width in order to resolve the "left-right" ambiguity. The chambers will be mounted on a frame of octagonal (or hexagonal) shape.

We also explore a possibility of using frames having a form of a closed semi-circle. The detection planes would consist of pairs of such frames put together along the common diameter. These frames could be mounted and dismounted without necessity of removing the beam-pipe.

3.3.4 Particle Identification

Particle identification (PID) for hadrons and leptons over a large range of solid angle and momenta is an essential requirement for meeting the physics objectives at the *HESR*. Charged particles in a medium

with index of refraction n, propagating with velocity $\beta c < 1/n$, emit radiation at an angle $\Theta_C = \arccos(1/n\beta)$. Thus, the mass of the detected particle can be determined by combining the velocity information determined from Θ_C with momentum information from the tracking detectors. Due to the strong variation of the typical particle momentum with polar angle, the particle identification can be achieved by two types of ring imaging Cherenkov counters (RICH) in the TS with different values of n.

Detector of Internally Reflected Cherenkov Light Within the TS, at polar angles between 22°-140°, particle identification can be performed by the detection of internally reflected Cherenkov (DIRC) light as realized in the *BaBar* detector [82]. It consists of 1.7 cm thick quartz slabs (n=1.544) surrounding the beam line at a radial distance of 48 cm. The main costs of the *BaBar* setup arise from the 11000 photomultiplier tubes, which allow timing information to be used to suppress the large background resulting from the electron beam environment. At $\overline{\mathsf{P}}$ANDA, these costs could be reduced by employing by employing new optical readout schemes e.g. with APD arrays or by replacing one of the two space dimensions for the Cerenkovrings by the timing information (see chapter A.1.2 for details). in the next detector shell.

Aerogel Cherenkov Counter Aerogel Cherenkov Counters (ACC) with a refractive index of $n = 1.02$ provide PID and information for higher-level triggers, and are located in the end-cap of the TS between polar angles of 5°-22°. They are especially suited for π-K separation. The optical transmission (re-scattering) limits the thickness of the blocks to about 4 cm. The measurement of the light cones by exploiting proximity focusing at 10 cm from the exit of the radiator with multi-pad gas detectors allows a compact construction without mirrors and Photomultiplier-tubes. With this geometry photons from asymptotic particles are found on rings of 24±4 mm radius. The concept of an aerogel RICH is included in the *LHCb* detector, and the high quality aerogel is already being used by the *Belle* collaboration [83]. Since the Rayleigh scattering of the Cherenkov photons in the radiator increases strongly with frequency, a R&D effort will be needed to develop materials for the photon converter that are sensitive to lower photon frequencies than measurable with CsI. As a fall-back solution, the geometry can be slightly modified so that a mirror reflects the light onto photomultipliers outside of the magnetic field region. The solution would however be significantly more expensive.

Muon Detection The muon detection (MUD) in $\overline{\mathsf{P}}$ANDA is a delicate task due to both the very low cross section of the interesting channels compared to muons from the decay of pions which are abundantly produced in $\overline{\mathsf{p}}$p annihilation.

Behind the iron yoke of the TS, plastic scintillator counters for muon detection will be installed that cover the laboratory polar angular range from 80° down to the opening for the dipole. Coverage to larger polar angles is not needed since the muons will be stopped in the iron yoke. The momentum of those muons is determined by the TS-tracking. The TS-MUD system will consist of about 96 individual bars that are 10 cm wide, 2 cm thick and about 2 m long. In addition there is an equal number of bars perpendicular to the beam axis, at the front of the TS-solenoid. The bars are read out with photomultipliers fed to ADCs and TDCs. This information can be used to determine the position for matching with the TS-tracking, and the time of flight, to suppress random coincidences. The energy information provides not only a redundant position information, but also a value of dE/dx to permit further background suppression.

3.3.5 Electromagnetic Calorimeter

Expected high count rates and a geometrically compact design of the target spectrometer require a fast scintillator material with a short radiation length and Moliere radius for the construction of the electromagnetic calorimeter (EMC). In recent years $PbWO_4$ has been proposed and confirmed as a high density inorganic scintillator with sufficient energy and time resolution for photon, electron and hadron detection even at intermediate energies [84]. For high energy physics $PbWO_4$ has been chosen by the *CMS* and *ALICE* collaborations at *CERN* [85] and optimized for large scale production. Besides a short decay time of less than 10 ns good radiation hardness has been achieved [86]. Recent developments indicate a significant increase of light yield due to crystal perfection and appropriate doping to enable photon detection down to 10 MeV with sufficient resolution. Optional cooling down to -25°C can further increase the light yield by a factor 3–4 compared to room temperature operation. It is proposed to use crystals of approximately 20 X_0 in length achieving an energy resolution below 2 % at 1 GeV [84] at a tolerable energy loss due to longitudinal leakage of the shower. These crystals allow π-e discrimination of 10^3 for momenta above 0.5 GeV/c. Therefore, particle identification does not rely on an additional gas

Cherenkov detector in favor of a very compact geometry. Tapered crystals with a front size of $2.2\times2.2\,\text{cm}^2$ mounted with an inner radius of 50 cm will be used. This implies 12000 crystals for the barrel part of the calorimeter. The backward and forward end-caps will comprise additional 3000-4000 modules. The readout of the crystals will be accomplished by large area avalanche photodiodes with optimized light collection, a tolerable nuclear counter effect and a fast timing information.

3.3.6 Target Spectrometer Solenoid

The target solenoid consists of a superconducting coil with an inner radius of 90 cm and a length of 2.5 m. The maximum magnetic field is 2 T. The field homogeneity is better than 5 % over the volume of the inner and outer tracker. In order to minimize the amount of material in front of the EMC, the latter is placed inside the magnetic coil. The bending power downstream of the target allows a reasonable momentum resolution even at the smallest polar angles (5°) detected only in the solenoid. This minimum angle of the solenoid acceptance is small enough to allow the dipole magnet to maintain a 1 m gap height. The cryostat for the coils has two warm bores of 100 mm diameter one on top and the other on bottom of the target position to allow for insertion of internal targets.

3.3.7 Germanium Detectors for γ Spectroscopy

The hypernuclei study will make use of the modular structure of $\overline{\text{P}}$ANDA. Removing the upstream part of the calorimeter will enable us to add a second nuclear target station and the required additional detectors close to the entrance of $\overline{\text{P}}$ANDA. The hypernuclear measurements will comprise three basic components: a) Detection of anti-hyperons and low momentum K^+ in the forward region. While the anti-hyperons will be detected with the universal detector, the kaon detection requires a time of flight measurement because of the low momenta of the kaons. b) A compact high resolution solid state tracker for absorption and tracking of low momentum hyperons at large angles. The geometry of this secondary target is determined by the short mean life of the Ξ^- of only 0.164 ns. This limits the required thickness of the active secondary target to about 25–30 mm. It will consist out of a compact sandwich structure of micro strip detectors (as used for the MVD) and absorbing material. c) High resolution and highly efficient Ge-array for γ-ray detection. Here we will make use of the large volume Ge-arrays presently under construction at *GSI* [87]. The main limitation will be the load due to neutral or charged particles traversing the Ge detectors. Therefore, we are presently developing readout schemes and tracking algorithms which will enable high resolution γ-spectroscopy in an environment of high particle flux.

3.4 Forward Spectrometer

3.4.1 Dipole Magnet

A superconducting dipole magnet of window frame type with 1 m gap and 2 m aperture will be used for the momentum analysis of charged particles in the forward spectrometer (FS) The magnet yoke will occupy the space between 4 m and 6 m downstream of the target and will define the angular acceptance of the FS to ±10° in the horizontal direction and ±5° in the vertical direction. The maximum bending power of the magnet will be 2 Tm and the resulting deflection of the antiproton beam at the maximum momentum of 15 GeV/c will be 2.2°. The iron yoke of this dipole magnet can be instrumented with detectors for ionizing particles. This option will become important for maximizing the muon detection efficiency. The beam deflection will be compensated by three correcting dipole magnets - two placed upstream and one downstream of the $\overline{\text{P}}$ANDA detection system.

3.4.2 Tracking Detectors

The deflection of particle trajectories in the field of the dipole magnet will be measured with a set of 4 drift chambers (MDC), 2 placed before and two behind the dipole magnet. The chambers will have rectangular frames with an active area of $1.3\times0.7\,\text{m}^2$ in the first chamber and $2.4\times1.2\,\text{m}^2$ in the second pair. The chambers will contain quadratic (or hexagonal) drift cells of 1 cm width, the same as in the TS-chambers. Each chamber will contain three pairs of detection planes: one pair with vertical wires and two pairs with wires inclined by +45° and -45° (or slightly smaller). This configuration will allow to reconstruct tracks in each chamber separately also in case of multi-track events. The beam-pipe will pass

through central holes in the chambers and the most central wires will be either eliminated or mounted on additional insulating rings surrounding the pipe. The expected momentum resolution of the system for 3 GeV/c protons is $\delta p/p$=0.2 % and is limited mainly by the small angle scattering on the chamber wires and gas.

3.4.3 Particle Identification

Time-of-Flight Detector The stop time-of-flight detector (TOF) will consist of a wall of tiles made of organic scintillator and read out on both ends by fast photomultipliers. The TOF will be measured between the start detector placed in the target region and the stop wall placed 6.8 m from the target. With the expected time resolution of σ=100 ps π-K and K-p separation on a 3 σ level will be possible up to momenta of 2.8 GeV/c and 4.7 GeV/c, respectively.

Ring Imaging Cherenkov Counter In order to extend the momentum range for the π-K and K-p separation beyond that of the TOF system we consider to use a dual-radiator RICH detector like the one developed for the *HERMES* experiment [88]. Using two radiators – silica aerogel and C_4F_{10} gas – with different indices of refraction equal to 1.0304 and 1.00137, respectively, provides π-K-p separation in a broad momentum range from 2–15 GeV/c. Due to the usage of a lightweight mirror which focuses the Cherenkov light on an array of photomultipliers placed outside the active volume, the total thickness of the detector is reduced to the freon gas radiator (5% X_0) , the aerogel radiator (2.8% X_0) and the aluminum window (3% X_0).

3.4.4 Calorimeter and Muon Detection

As a calorimeter for the forward region we consider to use the mid-rapidity calorimeter *MIRAC* from the *WA80* experiment. *MIRAC* consists of 30 independent stacks with the dimensions of 22 cm horizontally and 120 cm vertically. Each stack consists of a lead-scintillator electromagnetic section 15 X_0 long, and a steel-scintillator hadronic section 6 X_0 long. The energy resolution for electromagnetic and hadronic showers is $(0.014+0.11/\sqrt{E/GeV})$ % and $(0.034+0.34/\sqrt{E/GeV})$ %, respectively. At $\overline{\mathsf{P}}$ANDA the *MIRAC* stacks will be arranged in two rows - upper and lower one - covering an active area of 3 m in the horizontal and 2.4 m in the vertical direction. The stacks will occupy the space between 7 m and 9.14 m downstream of the target. The beam will go through a small slit between the upper and lower row of the most central stacks. The calorimeter will make it possible to measure besides energies of electrons and photons also energies of neutrons and anti-neutrons which are not registered in other components of the FS. Finally, behind the FS-calorimeter and the yoke of the dipole magnet there will be a wall of counters for muon identification similar to the ones in the TS.

3.5 Trigger and Electronics

3.5.1 Concept of FutureDAQ

In many contemporary experiments the trigger and data acquisition (DAC) system is based on a two layer hierarchical approach. A subset of especially instrumented detectors is used to evaluate a first level trigger condition. For the accepted events, the full information of all detectors is then transported to the next higher trigger level or to storage. The time available for the first level decision is usually limited by the buffering capabilities of the frontend electronics. Furthermore, the hard-wired detector connectivity severely constrains both the complexity and the flexibility of the possible trigger schemes. We aim at the development of a data acquisition concept which is much better matched to the high data rates and to the complexity of the next generation of experiments.

In our approach all detector channels are self triggering entities. They autonomously detect signals and pre-process them to extract and transmit only the physically relevant information. The data related to a particle hit, substantially reduced in the pre-processing step, is marked by a precise time stamp and buffered for further processing. The trigger selection finally occurs in so called compute nodes which access the buffers via a high bandwidth network fabric. The new concept provides a high degree of flexibility in the choice of trigger algorithms. It makes trigger conditions available which definitely are outside the capabilities of the standard approach, an obvious example being displaced vertex triggering.

In addition, all sub-detectors can contribute to the trigger decision on the same footing, and there are no restrictions due to hard-wired connectivity. Different physics can be accessed either in parallel or after software reconfiguration of the system.

3.5.2 Implementation Plan

Key technologies to be exploited within the DAQ framework are high speed serial (10 GBit/s per link and beyond) and high-density FPGA (field programmable gate arrays) with large numbers of programmable gates and more and more advanced embedded features. In the 3 years starting from 2004 the FutureDAQ project will deal with three major ingredients of the new architecture:

1. The basic building blocks of the hardware infrastructure, which can be combined in a flexible way to cope with varying demands, are the following:
   - Intelligent front-end modules capable of autonomous hit detection and data pre-processing (e.g. clustering, hit time reconstruction, pattern recognition) are needed. A generic sampling ADC module will be developed to be used e.g. for calorimeters and muon chambers.
   - A very precise time distribution system is mandatory to provide a clock normal from which all timestamps can be derived. Without this, data from subsystems can not be correlated.
   - Buffered data links provide point-to-point communication, typically via optical links, buffering and on-the-fly data manipulation.
   - Compute nodes aggregate large amounts of computing power in a specialized architecture rather then through commodity PC hardware. They may employ FPGAs, DSPs (digital signal processor) or other computing units and have to deal with feature extraction, association of data fragments to events and finally event selection.
2. A major component providing the glue between all others is the network fabric. Here special emphasis lies in cascadeable embedded switches which can be reconfigured to reroute traffic for different physics selection topologies.
3. Finally, the various algorithms for front-ends and selection levels have to be developed and tested. It should be attempted to develop a common high level programming environment for all components so that algorithms can be coded by physicists rather than engineers in more abstract programming languages than HDL and DSP assembler.

After implementing 1–3 a final evaluation of technologies and schemes will take place leading to a prototype design of the $\overline{\text{P}}$ANDA DAQ and trigger system to be completed by the end of 2008. This will be followed by a 1–2 year mass production and deployment phase.

4 Physics Performance

In order to demonstrate that the detector concept described above has sufficient sensitivity to measure the reactions discussed in the physics section, the acceptance and resolution of the detector system, as well as background rejection power has been estimated with simulations. After describing the simulations software package, results from three benchmark reactions are presented. These reactions have been chosen to demonstrate various main aspects relevant to the envisioned physics program.

If not stated otherwise, masses, widths and cross sections or branching fractions are taken from the most recent review of particle properties [89].

4.1 Overview of the Software Framework

The software framework has been devised with four major applications for events generation, simulation, reconstruction and final analysis. Four-momentum vectors of all particles leaving the reaction zone are generated. Several different event generators depending upon the process of interest are available. In order to determine the feed-through from the remaining annihilation channels, the Dual Parton Model is used as a background generator [90]. Similarly, the feedthrough from background events in $\overline{\text{p}}A$ annihilation reactions is calculated using the UrQMD model [91, 92]. Specific (signal) channels from $\overline{\text{p}}$p

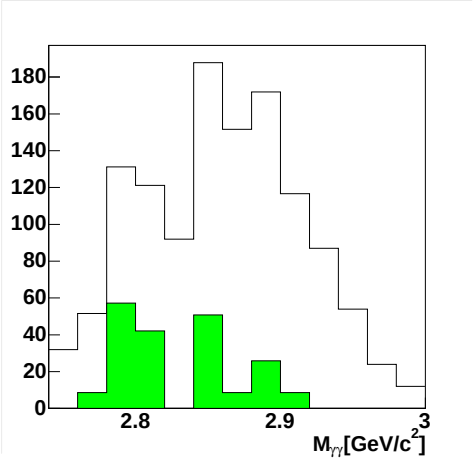

Figure 4: $\gamma\gamma$ invariant mass distribution for events with exactly two photon candidates. The solid curve shows simulated events of the reaction $\overline{\mathrm{p}}\mathrm{p} \to \eta_c \to \gamma\gamma$. The curve denoted by the filled area corresponds to the background events of the types $\pi^0\pi^0$ and $\pi^0\gamma$. The vertical scale denotes the number of events per 20 MeV/c^2 bin for 10,000 generated η_c events.

annihilation are efficiently calculated with a module using the appropriate angular momentum weighted phase factors and mass dependent widths and are added to the event stream [93]. These particles and all subsequently produced secondaries are tracked through the detector volume using GEANT4 [94]. They are reconstructed to composite information such as clusters in the EMC or tracks in the MVD, STT and MDCs. Finally this information is combined to particle candidates which are subject to the physics analysis. The software framework including the communication is based on ROOT [95]. Due to limitations of computing resources, the background has been scaled to the correct value relative to the signal for all three performance checks discussed below. Since the final background yield is small, statistical fluctuations may create peak-like structures in the up-scaled histograms.

4.2 Photon Final States: $\overline{\mathrm{p}}\mathrm{p} \to \eta_c \to \gamma\gamma$

The ability of the EMC to extract weak signals in events with purely photon final states has been studied by simulating the reaction $\overline{\mathrm{p}}\mathrm{p} \to \eta_c \to \gamma\gamma$. This signal has been observed with a maximum peak-to-background ratio of about 1 to 1 by the *E835* experiment [8] in the kinematic range $|\cos\theta^*| < 0.25$ (θ^* being the angle between the direction of the photon in the CM frame and the beam). The main sources for background to this signal with a formation peak cross section of about $\sigma_{\eta_c} \approx 200$ pb are the reactions $\overline{\mathrm{p}}\mathrm{p} \to \pi^0\gamma$ and $\overline{\mathrm{p}}\mathrm{p} \to \pi^0\pi^0$ where one or two low energetic photons may get lost and are thus identified as two photon final states [96]. Their production cross sections for $|\cos\theta^*| < 0.25$ are $\sigma_{\pi^0\gamma} \approx 2.5$ nb and $\sigma_{\pi^0\pi^0} \approx 25$ nb respectively . Backgrounds are assumed to be isotropic which is a reasonable approximation in this limited kinematic range. $\sigma_{\eta_c} \approx 50$ pb was chosen for the η_c signal since it's a pseudoscalar with a flat angular distribution. In order to compare with the *E835* results, this analysis is also limited to the same $|\cos\theta^*|$ range.

Events with two photons have been selected by requiring that no charged particles have been observed, and that there are exactly two clusters from neutral particles in the EMC. The remaining event sample is still dominated by the background channels mentioned above. To further reduce the background contribution, the missing mass squared of the final state was required to be less than 0.16 GeV$^2/c^4$, and the cosine of the CM angle between the two photons was required to be $\cos\theta_{\gamma\gamma} <$ -0.9999. In addition, the cosine of the angle between the CM system and the beam was required to be $|\cos\theta_{CM}| < 0.25$. The invariant mass distribution for events with two photon candidates is shown in figure 4. The solid line indicates events only from the decay of the η_c and the filled area represents feedthrough from events of the type $\pi^0\pi^0$ and $\pi^0\gamma$. Due to the good coverage of the backward hemisphere, there is almost no background left from $\pi^0\pi^0$ and the residual background originates mostly from $\pi^0\gamma$. From these results, the reconstruction efficiency for the η_c channels is determined to be 10.3 %. Furthermore, the signal-to-background ratio is about (5.1±0.4):1, significantly better than the result obtained by *E835*.

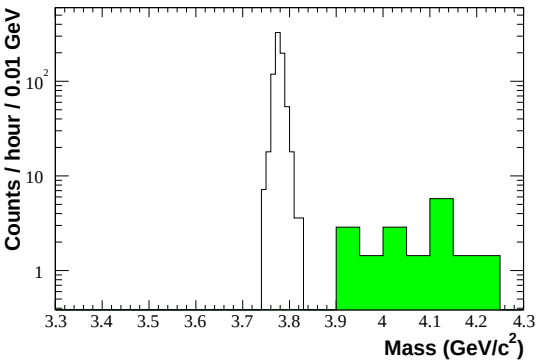

Figure 5: Mass difference between the $D\overline{D}$ and the two D candidates plus their nominal masses. The vertical scale denotes the number of observed counts per 10 MeV/c^2 bin per hour of measuring time. The filled histogram corresponds to the background events and the solid histogram is the sum of signal plus background.

4.3 Open-Charm: $\overline{\text{p}}\text{p} \rightarrow \psi(3770) \rightarrow D\overline{D}$

The capability of the MVD to select displaced vertices from the decay of D mesons has been investigated by evaluating the $D^{\pm} \rightarrow K^{\mp}\pi^{\pm}\pi^{\pm}$ decay channel produced in the reaction $\overline{\text{p}}\text{p} \rightarrow \psi(3770) \rightarrow D^{+}D^{-}$. Very high selectivity is needed here because this final state is suppressed by about a factor 10^7 relative to the total annihilation cross section.

D meson candidates are selected by performing a constrained fit of all sets of three unequal sign tracks (i.e. $++-$ or $--+$) to a common vertex. Candidates with an invariant mass consistent with a D meson, as well as a fit quality of $\chi^2/\nu < 10$ (ν=number of degrees of freedom) and the z component of the vertex $V_z > 0.15$ mm resulting from a constrained fit have been selected for further evaluation. The missing mass (M_{miss}) has been calculated for those events with exactly one D^+ and one D^- candidate. After requiring that $M^2_{miss} < 0.001\,\text{GeV}^2/c^4$ the helicity angle θ^* has been calculated. θ^* being the angle between the CM momentum vector of the D^+ candidate and the beam axis. Due to an asymmetry of this variable for the background events, an improvement of the signal-to-background ratio can be obtained by requiring $\cos\theta^* >$-0.7. A better resolution for the $\psi(3770)$ is achieved by using a mass difference measurement between the $D\overline{D}$ candidate and the two D candidates. This is shown in figure 5 While the signal-to-background ratio using an invariant mass distribution is 6:1, the background moves away from the signal in the mass difference measurement so that within the given statistics there is no background left under the $D\overline{D}$ signal. The filled histograms show the distribution for background events, and the solid histograms show the sum of signal and background events. The total efficiency for this channel is about 25 % over the full range of $\cos\theta^*$ and about 20 % for the range used here. This analysis shows that the signal can be extracted with very low background. Significant further improvements can be expected by including the kaon identification into the analysis chain, and by correctly accounting for small angle scattering and energy loss of the particles in the detectors.

4.4 Muon Pairs in Nuclear Reactions

One of the basic trigger concepts of the $\overline{\text{P}}$ANDA detector is based on the decay of heavy resonances in light particles with large transverse momenta, e.g. the decay of J/ψ in two muons. This enables triggering on two muons with large transverse momenta in the presence of muons from hadronic background. The detection of J/ψ mesons produced in $\overline{\text{p}}A$ collisions on nuclear targets serves here as an example to study the production of J/ψ production in nuclear matter. In Fig. 6 the invariant mass of two muons detected solely in the muon counters of the target spectrometer is plotted for an integrated luminosity of 180 nb^{-}1. For all muon candidates, track parameters and hit locations within the detectors are required to fulfill the condition of having a muon probability of more than 95 %. The signal peak at the invariant mass of the J/ψ represents calculations from [93] for $\overline{\text{p}} + ^{63}Cu$ at 4.05 GeV/c after a filter procedure. The target spectrometer alone detects 45 % of the originally produced J/ψ. This peak is well separated from nuclear background events which were calculated using the UrQMD [91] event generator. These entries are the combinatorical background of muons coming from the decay of resonances of light quark mesons, especially from misidentified pions. From this study we conclude that the large transverse energies of the muons allow the reconstruction and the identification of J/ψ mesons within a nuclear background which

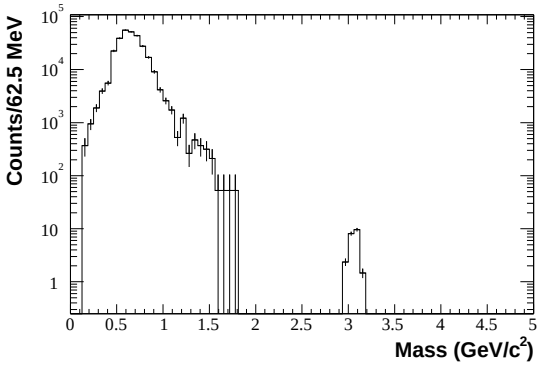

Figure 6: Invariant mass spectrum of J/ψ decaying in two muons. The signal at $3\,\mathrm{GeV}/c^2$ is from calculations in [93], the combinatorical background at lower invariant masses is taken from UrQMD calculations [91].

is 10^3-10^4 stronger than the signal.

5 Implementation

5.1 Experimental Area

The target for antiproton physics is located in the straight section at the east side of the *HESR*. At this location an experimental hall of 35.0×23.5 m floor space and 14.0 m height is planned (see figure 7). On both sides along the beam line a concrete radiation shield of 2 m thickness is built up which is covered by bars of 1 m thickness to suppress the neutron sky shine. Within this elongated concrete cave the $\overline{\mathrm{P}}$ANDA detector together with auxiliary equipment and beam steering and focusing elements will be housed. The roof of the cave can be opened by crane to access heavy components. The target spectrometer of $\overline{\mathrm{P}}$ANDA

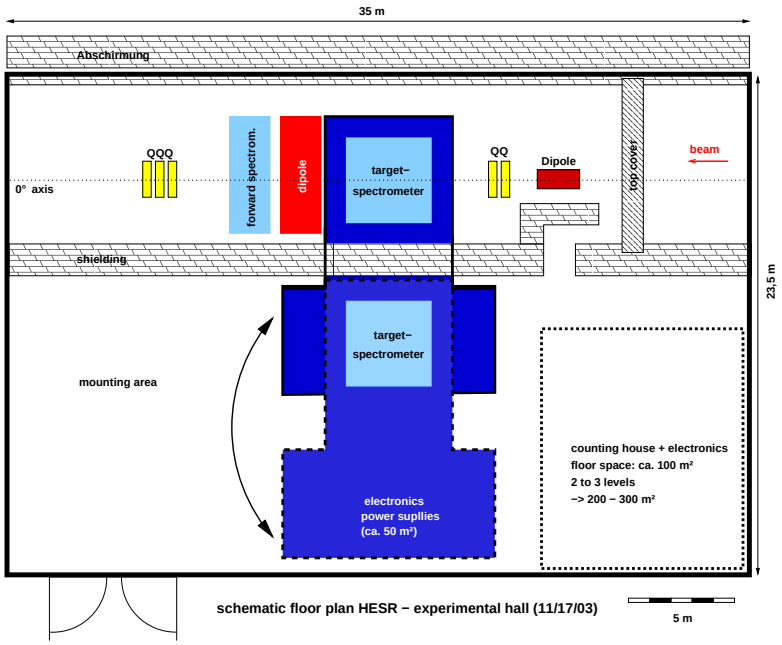

Figure 7: Experimental area.

with electronics and supplies should be mounted on a carriage which makes it retractable to a parking position outside the *HESR* beam line. The experimental hall has space on the left side of the parking position for delivery of components and assembly of the detector whereas to the right a counting house with two or three floors can be installed. The crane (30 t) spans the whole area with the hook at the height of 10 m.

Sufficient (300 kW) electric power will be mounted. Liquid helium coolant may come from the main cryogenic liquefier for the *SIS* rings. Alternatively, a separate small liquefier (50 W cooling power at 4 K) will be available. The temperature of the whole building will be moderately controlled. The more stringent requirements with respect to temperature and humidity for the detector has to be maintained locally in the vicinity of $\overline{\text{P}}$ANDA.

There is the request for 600 m^2 additional laboratory and office space located in the nearby operations building as well as a conference room.

5.2 Radiation Environment

Radiation safety of the experimental cave has extensively studied with the Fluka code [97]. It turns out that a shielding along the beam line with 1 m thickness of concrete is sufficient. The sky shine can be suppressed with 0.5 m concrete blocks.

5.3 Organization and Responsibilities

The workload required in the development and building of all components of the $\overline{\text{P}}$ANDA detection system, including the read-out electronics and data acquisition system, is shared among the institutions listed at the beginning of this Letter of Intent. Each of the participating groups has expressed its strong interest to deliver a sizeable contribution to the $\overline{\text{P}}$ANDA setup. For some of the participating institutions this would require a redefinition of the priorities within their research program, and a major rearrangement of their resources in terms of investment and personnel. The process of defining the longer term research activities related to the $\overline{\text{P}}$ANDA project is presently not completed, partially due to open questions concerning financial support in the intermediate future. The list of institutions associated to the various detector components has therefore to be understood as an expression of interest of these institutions in the respective technical issues on the basis of the existing expertise and infrastructure. The commitment of each of the participating institutions concerning its contribution to the PANDA project will be defined in a Memorandum of Understanding in the near future. A preliminary distribution of tasks is given below:

Pellet target
GSI, FZ Jülich, TSL Uppsala, U Uppsala

Cluster-jet target
GSI, U Münster, U/INFN Genova, IMEP Vienna

Superfluid He-target
U Frankfurt

Nuclear targets
FZ Jülich

Micro vertex detector
U Catania, TU Dresden, U Edinburgh, GSI, FZ Jülich, U Mainz, INFN Torino, U Torino ("Dep.Exp.Phys.")

Cylindrical tracker - STT/TPC
JINR Dubna, LNF Frascati, INFN Ferrara, GSI, FZ Jülich, IMP Lanzhou, TU München, U Tübingen, U Uppsala

Particle identification - DIRC/RICH/TOF
U Catania, JINR Dubna, U Gießen, U Glasgow, GSI, FZ Jülich, IMEP Vienna

Electromagnetic calorimeter - EMC
U Bochum, U Gießen, GSI, KVI Groningen, FZ Jülich, IMP Lanzhou, U Mainz, U Minsk, TU München, U Stockholm, U Uppsala, SINS Warsaw

Magnet
U Cracow, JINR Dubna, U/INFN Genova, U Glasgow, IMP Lanzhou

Muon chambers - MUD
JINR Dubna, GSI, U Piemonte Orientale, INFN Torino, U Torino ("Dep.Gen.Phys.")

Forward spectrometer - FS
U Cracow, JINR Dubna

Ge-Detector
U/INFN Catania, Politecnico Torino, U Mainz, KTH Stockholm, INFN Torino , U Torino ("Dep.Exp.Phys.")

DAQ/Trigger/Fast electronics
U Cracow, U Gießen, GSI, FZ Jülich, U Katowice, U Milano, TU München, U Pavia, INFN Torino, U Torino ("Dep.Gen.Phys."), SINS Warsaw

Computing
U Bochum, U Bonn, U Glasgow, GSI, FZ Jülich, U/INFN Pavia, TU München, Politecnico Torino, SINS Warsaw

5.4 Time Schedule

Fig. 8-9 show the estimated schedule from R&D to commissioning of the various techniques and components for a prospected roll-on at the end of 2011. This implies a start of installation in the *HESR* experimental hall in 2009.

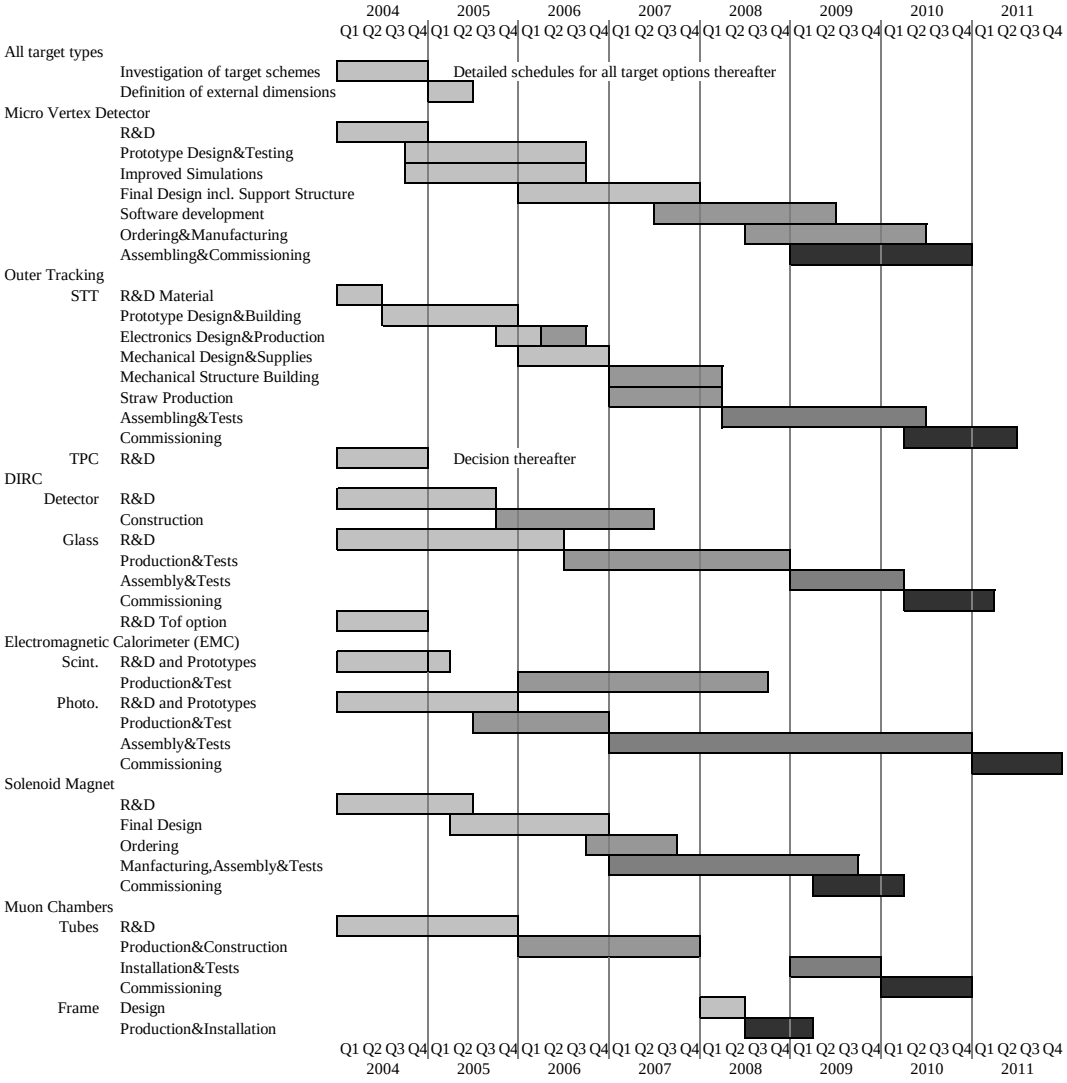

Figure 8: Time schedule for the design, construction and commissioning of the $\overline{\text{P}}$ANDA Detector (Part I).

5.5 Beam Time Considerations

One run period is considered to have a length of 6–9 months ($\approx 1.5 \times 10^7$s). Depending on the nature of the experiment (slow or quick changes of beam momenta), the different filling/cooling-cycle schemes, and

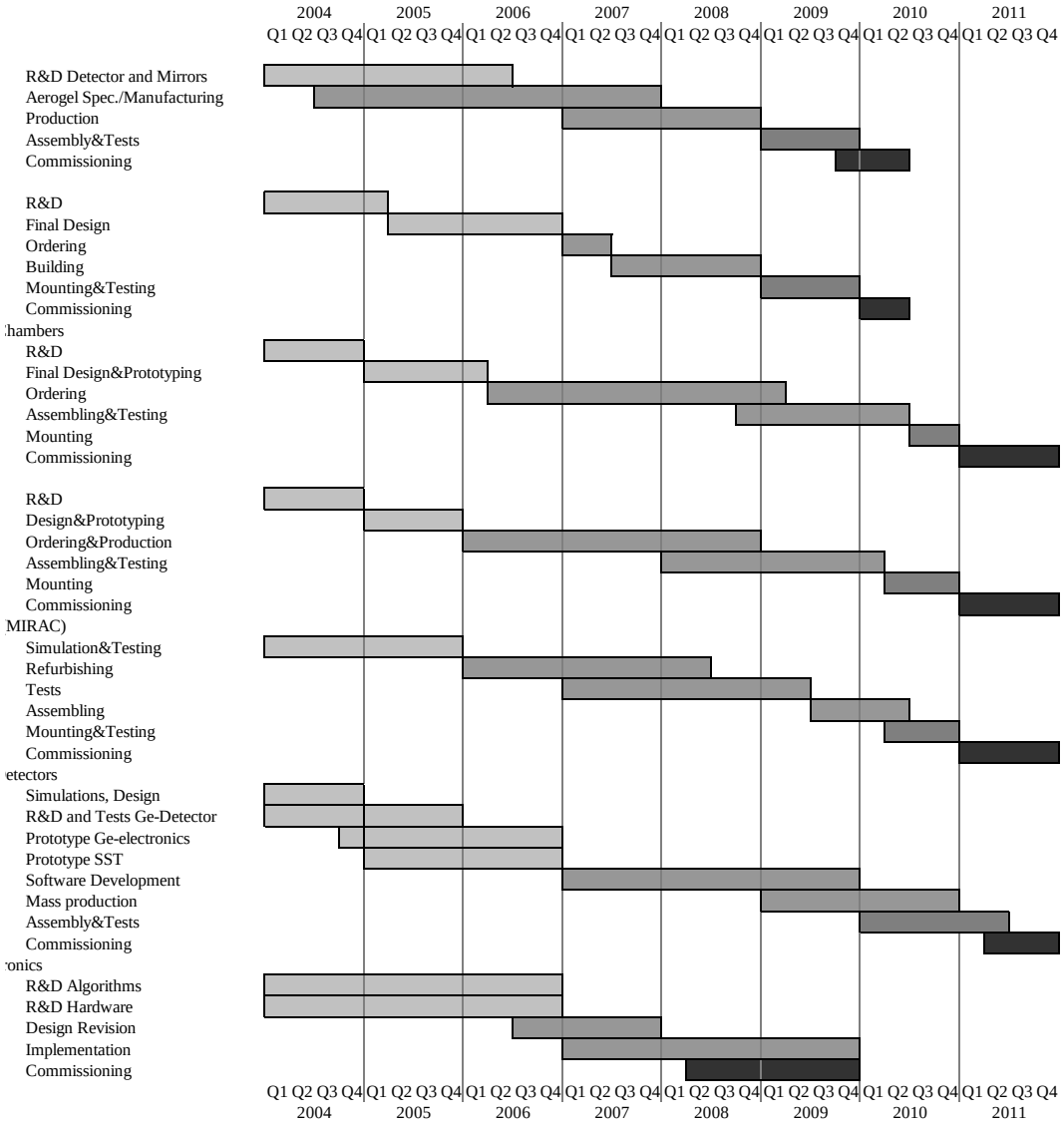

Figure 9: Time schedule for the design, construction and commissioning of the $\overline{\text{P}}$ANDA Detector (Part II).

other dead-times during data-taking the overall data-taking efficiency is expected to vary between 50 % (several changes a day) and 80 % (continuous running).

The key experiments charmonium study, charmed hybrid search, charm in nuclei, and hypernuclear physics are mutually exclusive and will require dedicated running for more than one (most probable two) full run period each. For charmonium and charmed hybrids this number is deduced from typical cross sections in the order of 10-100 pb and the minimum number of 1 k (per charmonium state) and 10–100 k (charmed hybrid) signal events for a conclusive analysis.

..arguments for the other two topics go here...

Optional measurements are performed simultaneuously together with the key experiments with identical beam and detector settings. E.g. the long data-taking run for charmed hybrids at the highest beam momentum will allow for mesasurements on electromagnetic processes.

Including a full start-up run period to tune and understand the detector and to measure unknown cross sections the initial program adds up to eight years of data taking. Most likely this number will change, since most measurements are explorative with badly known cross sections. One may also keep in mind that this is an active research field and the relevance of some of the proposed topics may have altered while others may come up in addition.

A Appendix

A.1 Supplements and Options

A.1.1 Tracking System

An interesting option for the central tracking detectors is provided by a high-rate time projection chamber, located inside the solenoid magnetic field between the MVD and the EMC replacing the STT (Section 3.3.3). Owing to the beam properties at the *HESR*, the chamber has to operate in cw mode, i.e. no gating is possible. The development of such an innovative device constitutes a challenge, both scientifically and technologically, and would lead to a novel detector beyond the current state-of-the-art tracking devices.

A time projection chamber with its low material budget constitutes an ideal device for tracking charged particles in 3-dimensional space. An open question, however, is the operation of such a chamber in a quasi-cw beam, where no gating is possible to suppress feedback of positive ions into the drift volume, an effect which would modify the electric field inside the drift space and thus spoil the drift time measurement. First studies in the framework of the time-projection chamber (TPC) currently under development for the *TESLA* experiment at *DESY* [98] indicate that novel micro-pattern gaseous detectors provide a promising alternative to a conventional read-out employing wires, possibly without gating due to a suppression of ion feedback intrinsic to these devices. One option here is the use of the GEM (Gas Electron Multiplier) [99], which has been invented recently at *CERN*.

Due to the configuration of the electric field, positive ions created in the GEM holes are mainly disposed at the top GEM electrode. For cw-operation of a TPC, however, the ion feedback has to be suppressed below 1-2 %, a challenge which requires careful optimization of field configurations and geometries. In addition, the feedback of ions into the drift volume might be further suppressed by inserting a GEM foil with gain 1, which is fully transparent to electrons, but almost opaque for ions.

A.1.2 Particle Identification

Time-of-Flight Detector To allow the identification of low momentum particles, a scintillating start detector may have to be placed between the DIRC and the straw tubes. The mechanical support of the DIRC can be used for the TOF barrel, which should have the same length as the DIRC panels. Two different versions have been discussed, each consisting of panels with a rectangular shape of $4.4\times1\,\mathrm{cm}^2$. Since readout cannot be done in the forward direction, either a single layer barrel should be used, where the time can only be calculated after the tracking, or a double helix structure, where the z-Position is determined by the overlapping region of two helices with the different rotational direction. More R&D is needed to find the best solution for such scenario.

Alternative DIRC Concepts The main drawback of the DIRC concept (Section 3.3.4) is the large size of the required photon detectors and the very limited particle identification capability below 600 MeV/c momentum. By exploiting the dependence of time-of-propagation (TOP) of Cherenkov light on the Cherenkov angle the measurement of one position coordinate in the DIRC concept is replaced by a time measurement. This significantly reduces the size of the photon detector of the RICH detector. Presently this idea is pursued by the *BELLE* collaboration for a future upgrade [100, 101]. Furthermore, the time-of-flight detector needed as a start detector for the TOP measurement will allow to extend the PID to lower momenta.

Muon Detection The reconstruction of and triggering on muons can be significantly improved by additional tracking detectors replacing the MUD (Section 3.3.4). The basic element could be the metallic cathode Iarocci-like 8-cells profile drift tube (called mini drift tubes (MDT)) with a cell cross section of $9.4\times9.4\,\mathrm{mm}^2$ and a wall thickness of 0.6 cm. Similar tubes, in operation at *COMPASS* and at *D0*, feature a spatial accuracy better than 1 mm. The longitudinal coordinate is obtained by the induced charge on strips glued on MDTs and equipped with FADCs. The expected accuracy is better than 200 μm.

The TS muon detector will then cover an angular range of $\approx 22°$-$90°$. It will be composed of an inner barrel (4 planes) and an outer barrel (6 planes) sandwiching the iron yoke of the target solenoid and an end-cap (4 planes) perpendicular to the beam axis with a central hole.

For the muon detection in the forward spectrometer (angular range covered $\approx 10°$-$22°$) stations will be

mounted at the outer and rear sides of the dipole magnet, exploiting the yoke of the magnet as a muon filter. To cover the very forward region up to $\approx 10^\circ$ we may use 3 stations of muon detectors (4, 4, 6 planes, respectively), the first two in the region of the hadron calorimeter and the last one behind it.

References

[1] L. Äystö *et al.*, An International Accelerator Facility for Beams of Ions and Antiprotons, Conceptual Design Report, *GSI*, 2001.

[2] Letter of Intent: Construction of a Glue/Charm-Factory at *GSI*, 1999 `http://www.ep1.ruhr-uni-bochum.de/gsi/part1.ps.gz`.

[3] *HESR*-Project, Contributions to the Scientific Case, 1999 `http://www.ep1.ruhr-uni-bochum.de/gsi/part2.ps.gz`.

[4] K.K. Seth, Proceedings of Heavy Flavours 8, Southhampton, UK, 1999.

[5] S.-K. Choi, S.L. Olsen *et al.*, Phys. Rev. Lett. **89** (2002) 102001.

[6] G. Wagner *et al.*, hep-ex/0305083; J. Ernst *et al.*, hep-ex/0306060.

[7] C. Edwards *et al.*, Phys.Rev.Lett. **48** (1982) 70.

[8] F. Fang, T. Hojo *et al.*, Phys. Rev. Lett. **90** (2003) 071801; M. Andreotti *et al.*, Phys. Lett. B **566** (2003) 45; B. Mayer, private comm.

[9] J. Pantaleone, S.-H. Tye, Phys. Rev. D **37** (1988) 3337; S.N. Gupta,W.W. Repko, and C.J. Suchyta, Phys. Rev. D **39** (1989) 974; V.V. Dixit, V. Gupta, and R. Kögerler, Phys. Rev. D **42** (1990) 166; A.M. Badalyan and V.P. Yurov, Phys. Rev. D **42** (1990) 3138; L.P. Fulcher, Phys. Rev. D **44** (1991) 2079; J. Stubbe, and A. Martin, Phys. Lett. B **271** (1991) 208.

[10] D. Bettoni, private comm.

[11] T.A. Armstrong *et al.*, Phys. Rev. D **48** (1993) 3037.

[12] M. Ambrogiani *et al.*, Phys. Rev. D **62** (2000) 052002.

[13] J.Z. Bai *et al.*, Phys. Rev. D **57** (1998) 3854.

[14] L. Antoniazzi *et al.*, Phys. Rev. D **50** (1994) 4258; R. Brandelik *et al.*, Phys. Lett. B **76** (1978) 361; J.L. Siegrist *et al.*, Phys. Rev. Lett. 36 (1976) 700.

[15] S.-K. Choi *et al.*, subm. to Phys. Rev. Lett., hep-ex/0309032.

[16] D. Acosta *et al.*, subm. to Phys. Rev. Lett., FERMILAB-PUB-03/393-E.

[17] D.R. Thompson *et al.*, Phys. Rev. Lett. **79** (1997) 1630.

[18] G.S. Adams *et al.*, Phys. Rev. Lett. **81** (1998) 5760.

[19] A. Abele *et al.*, Phys. Lett. B **423** (1998) 175.

[20] J. Reinnarth, Nucl. Phys. A **692** (2001) 268c.

[21] C. Amsler *et al.*, Phys. Lett. B **B342** (1995) 433; C. Amsler *et al.*, Phys. Lett. B **353** (1995) 571; A. Abele *et al.*, Phys. Lett. B **385** (1996) 425; A. Abele *et al.*, Eur. Phys. C **19** (2001) 667; C. Amsler *et al.*, Phys. Lett. B **340** (1994) 259.

[22] P. Chen, X. Liao, and T. Manke, Nucl. Phys. Proc. Suppl. **94** (2001) 342.

[23] C. Michael, Proceedings of Heavy Flavours 8, Southampton, UK, 1999.

[24] R. Cester, Proceedings of the 'Super *LEAR* Workshop', pp. 91-103, Oct. 1991, Zurich.

[25] M.K. Gaillard, L. Maiani and R. Petronzio, Phys. Lett. B **110** (1982) 489.

[26] C.J. Morningstar, M. Peardon, Phys. Rev. D **60** (1999) 034509

[27] J. Sexton, A. Vaccarino, and D. Weingarten, Phys. Rev. Lett. **75** (1995) 4563.

[28] P.R. Page, Proceedings of the 'pbar2000 Workshop', edited by D.M. Kaplan and H.A. Rubin, Chicago, 2001, pp. 55-64; K. Peters, Proceedings of the workshop 'LEAP 2003', edited by R. Hayano, in print.

[29] R. Jones, Proceedings of the workshop 'Gluonic excitations', Jefferson Lab, May 2003, in print.

[30] A. Bertin *et al.*, Phys. Lett B **400** (1995) 187; A. Bertin *et al.*, Phys. Lett B **385** (1996) 493; A. Bertin *et al.*, Phys. Lett B **400** (1997) 226; C. Cicalo *et al.*, Phys. Lett B **462** (1999) 453; F. Nichitiu *et al.*, Phys. Lett B **545** (2002) 261.

[31] H. Geissel *et al.*, Phys. Rev. Lett. **88** (2002) 122301; H. Geissel *et al.*, Phys. Lett. B **549** (2002) 64; K. Suzuki *et al.*, nucl-ex/0211023.

[32] M. Nekipelov *et al.*, Phys. Lett. B **540** (2002) 207; Z. Rudy *et al.*, Eur. Phys. J. A **15** (2002) 303.

[33] Y. Shin *et al.*, Phys. Rev. Lett. **81** (1998) 1576; R. Barth *et al.*, Phys. Rev. Lett. **78** (1997) 4007; F. Laue *et al.*, Phys. Rev. Lett. **82** (1999) 1640.

[34] P. Crochet *et al.*, Phys. Lett. B **486** (2000) 6; K. Wisniewski *et al.*, Eur. Phys. J. A **9** (2000) 515.

[35] F. Klingl, N. Kaiser, and W. Weise, Nucl. Phys. A 624 (1997) 527.

[36] F. Klingl, S. Kim, S.H. Lee, P. Morath, and W. Weise, Phys. Rev. Lett. **82** (1999) 3396.

[37] S.H. Lee, and C.M. Ko, Phys. Rev. C **67** (2003) 038202; S.H. Lee, Proceedings of Int. Workshop 'HADRON 2003', Aschaffenburg, 2003, to be published.

[38] W. Weise, Proceedings of Int. Workshop 'Structure of Hadrons', Hirschegg, 2001.

[39] A. Hayashigaki, Phys. Lett. B **487** (2000) 96.

[40] A. Sibirtsev, K. Tsushima, and A.W. Thomas, Eur. Phys. J. A **6** (1999) 351.

[41] K. Seth, Proceedings of Int. Workshop 'Structure of Hadrons', Hirschegg 2001

[42] W. Cassing, Y. Golubeva, and L. Kondratyuk, Eur. Phys. J. A **7** (2000) 279.

[43] Ye.S. Golubeva, E.L. Bratkovskaya, W. Cassing, and L.A. Kondratyuk, Eur. Phys. J. A **17** (2003) 275.

[44] M. Danysz and J. Pniewski, Phil. Mag. **44** (1953) 348.

[45] M. Danysz *et al.*, Nucl. Phys. **49** (1963) 121.

[46] R.L. Jaffe, Phys. Rev. Lett. **38** (1977) 195; ibidem **38** (1977) 617(E).

[47] G.R. Farrar and G. Zaharijas, hep-ph/0303047 (2003).

[48] T. Sakai *et al.*, Prog. Theor. Phys. Suppl. **137** (2000) 121.

[49] T. Yamada and C. Nakamoto,Phys. Rev. C **62** (2000) 034319-1; K.S. Myint, S. Shinmura, Y. Akaishi, Eur. Phys. J. A **16** (2003) 21; I.R. Afnan and B.F. Gibson, Phys. Rev. C **67** (2003) 017001-1; I.N. Filikhin, A. Gal and V.M. Suslov, nucl-th/0303028 (2003).

[50] R.M. Sternheimer and M. Goldhaber, Phys. Rev. A **8** (1973) 2207; S.S. Gershtein and Yu.M. Zinov'ev, Yad. Fiz. **33** (1981) 1442; M.M. Giannini and M.I. Krivoruchenko, Phys. Lett. B **291** (1992) 329.

[51] Flair, `http://www-linux.gsi.de/~flair`.

[52] K. Goeke, M.V. Polyakov, and M. Vanderhaeghen, Prog. Part. Nucl. Phys. **47** (2001) 401.

[53] M. Diehl, habil. thesis, Univ. Hamburg (2003), hep-ph/0307382.

[54] D. Müller *et al.*, Fortschr. Phys. **42** (1994) 101; A.V. Radyushkin, Phys. Lett. B **380** (1996) 417.

[55] X.-D. Ji, Phys. Rev. Lett. **78** (1997) 610, hep-ph/9603249.

[56] A.V. Radyushkin, Phys. Rev. D **58** (1998) 114008, hep-ph/9803316.

[57] M. Diehl, Eur. Phys. J. C **8** (1999) 409, hep-ph/9811253.

[58] F. Close, and Zhao, Phys. Lett. B **553**, 2003, 211.

[59] A. Freund, A.V. Radyushkin, A. Schfer, and Ch. Weiss, Phys. Rev. Lett.**90** (2003) 092001.

[60] M. Diehl, P. Kroll, and C. Vogt, Eur. Phys. J. C **26** (2002) 567; M. Diehl, P. Kroll, and C. Vogt, Phys. Lett. B **532** (2002) 99.

[61] C.F. Berger, and W. Schweiger, Eur.Phys.J. C **28** (2003) 249.

[62] T.A. Armstrong *et al.*, Phys. Rev. D **56** (1977) 2509.

[63] M. Düren, Proc. X. Int. Conf. on Hadron Spectroscopy, Aschaffenburg, Germany (2003) to be published.

[64] G. Bunce *et al.*, Phys. rev. Lett. **36** (1976) 1113.

[65] V. Barone, A. Drago, and P.G. Ratcliffe, Rhys. Rep **359** (2002) 1.

[66] E. Annasontzis *et al.*, Phys. Rev. D **38** (1988) 1377.

[67] T.A. Armstrong *et al.*, Phys. Rev. Lett. **70** (1993) 1212; M. Ambrogiani *et al.*, Phys. Rev. D **60** (1999) 032002.

[68] B. Aubert *et al.*, Phys. Rev. Lett. **90** (2003) 242001.

[69] D. Besson, *et al.*, hep-ex/0305100; B. Krokovny *et al.*, hep-ex/0308019; Y. Mikami, *et al.*, hep-ex/0307052.

[70] N. Isgur, R. Kokoski, and J. Paton, Phys. Rev. Lett. **54** (1985) 869;

[71] M. Nowak, M. Rho, and I. Zahed, hep/ph/0307102; W. Bardeen, E. Eichten, and T. Hill, hep-ph/0305049.

[72] K. Abe *et al.*, hep-ex/0307021.

[73] I. Bigi, CP Violation, hep-ph/9712475, and Surveys High Energy Phys. **12** (1998) 269

[74] B. Aubert *et al.*, Phys. Rev. Lett. **87** 091801 (2001).

[75] K. Abe *et al.*, Phys. Rev. Lett. **87** 091802 (2001).

[76] G. Burdman, hep-ph/9407378, CHARM2000 Workshop, *FNAL* June 7-9, 1994

[77] P.F. Harrison and H.R. Quinn (Eds.), The *Babar* Physics Book, *SLAC*-R-504, 1998.

[78] C. Ekström, C.-J. Fridén, A. Jansson, J. Karlsson, S. Kullander, A. Larsson, G. Norman and the WASA Collaboration, NIM A **371** (1996) 572.

[79] The ATLAS Collaboration, ATLAS TDR 11, *CERN*/LHCC 98-13

[80] The CMS Collaboration, CMS TDR 5, *CERN*/LHCC 98-6

[81] P. Holl, P. Fischer, P. Klein, G. Lutz, W. Neeser, L. Strüder, N. Wermes, IEEE Trans. Nucl. Sc. Vol. **47** (2000) 1421.

[82] R. Aleksan *et al.*, Nucl. Instr. and Meth. in Phys. Res. A**397** (1997) 261.

[83] NIM A in preparation: `http://beauty.bk.tsukuba.ac.jp/belle/nim/total/`

[84] K. Mengel *et al.*, IEEE Trans. on Nucl. Sci. 45 (1998) 681; R. Novotny, R. Beck, W. Döring, V. Hejny, A. Hofstaetter, M.V. Korzhik, V. Metag, and H. Ströher, IEEE Trans. on Nucl. Sc. **47** (2000) 1499; M. Hoek *et al.*, Nucl. Instr. and Meth. in Phys. Res. A **486** (2002) 136

[85] ALICE Technical Proposal, *CERN*/LHC 9.71; CMS Technical Proposal, *CERN*/LHCC 94-38, LHCC/P1, 1994.

[86] E. Auffray *et al.*, SCINT99, Proceedings, Moscow, 1999.

[87] `http://www-dapnia.cea.fr/Sphn/Deformes/Agata/index.shtml`.

[88] N. Akopov *et al.*, Nucl. Instr. and Meth. in Phys. Res. A **479** (2002) 511.

[89] Review of Particle Physics, Phys. Rev. D **66** (2002) 1.

[90] V.V. Uzhinsky, and A.A. Galoyan, hep-ph/0212369.

[91] Prog. Part. Nucl. Phys. 41 (1998) 225.

[92] A.S. Galoyan, and A. Polanski, hep-ph/0304196

[93] M. Bleicher *et al.*, J. Phys. G **25** (1999) 1859; A. Sibirtsev, K. Tsushima, and A.W. Thomas, Phys. Rev. C **63** (2001) 044906.

[94] `http://wwwinfo.cern.ch/asd/geant4/geant4.html`

[95] see `http://root.cern.ch`

[96] M. Ambrogiani *et al.*, Phys. Lett. B **566** (2003) 45.

[97] see `http://www.fluka.org`

[98] The *TESLA* Collaboration, *TESLA*: Technical Design Report, *DESY* 2001-011, `http://tesla.desy.de/new\_pages/TDR\_CD/start.html`, 2001.

[99] F. Sauli, Nucl. Instr. Meth. **A386** (1997) 531.

[100] M. Akatsu *et al.*, Nucl. Instr. and Meth. A**440** (2000) 124.

[101] T. Ohshima, Nucl. Instr. and Meth. A**453** (2000) 331.